AN ABSTRACT OF THE DISSERTATION OF

Wesley D. Frey for the degree of Doctor of Philosophy in Radiation Health Physics presented on March 6, 2009.
Title: Use of BC-523a Liquid Scintillator for Simultaneous Neutron Spectroscopy and Gamma Counting with the Implementation of a Neutron History Reconstruction Algorithm.

Abstract approved:

_____

David M. Hamby

Real-time, high efficiency neutron spectroscopy has, historically, been a persistent challenge in the field of radiation detection and, for the most part, has gone unsolved. The most promising method to resolve this challenge, is the boron-capture technique using an organic scintillation system (BC-523a). Detectors that utilize this method possess an unusual property that allows them to be used for estimation of initial neutron energy over a large range of incident energies with very high intrinsic efficiencies. The two most significant problems with this method are that the recoil proton light response is non-linear (resulting in inaccurate neutron energy spectra) and the amount of analog circuitry required to process the pulses is prohibitive. This research resolves these two problems. The non-linear response is corrected by implementing a neutron history reconstruction algorithm. This algorithm tracks the theoretical amount of scintillation light generated by each neutron collision with

hydrogen. Neutron interactions that do not produce a measurable scintillation pulse (non-hydrogen collisions and inelastic scatter photons leaving the detector's active volume) will be characterized in MCNP, so that these signal losses can be accounted for. The majority of analog circuitry is replaced by a fast waveform digitizer and pulse processing program using digital filters. A plutonium beryllium neutron source was characterized. Results are available in real-time and are in good agreement with a historically accepted spectrum. Potential applications for this system include real-time mixed field dosimetry, neutron/gamma-ray sensitive portal monitors, and the possible replacement of the He-3 tube.

Use of BC-523a Liquid Scintillator for Simultaneous Neutron Spectroscopy and Gamma Counting with the Implementation of a Neutron History Reconstruction Algorithm

by

Wesley D. Frey

A DISSERTATION

submitted to

Oregon State University

in partial fulfillment of
the requirements for the
degree of

Doctor of Philosophy

Presented March 6, 2009
Commencement June 2009

Doctor of Philosophy Dissertation of Wesley D. Frey presented on March 6, 2009.

APPROVED:

_____

Major Professor, representing Radiation Health Physics

_____

Head of the Department of Nuclear Engineering and Radiation Health Physics

_____

Dean of the Graduate School

I understand that my thesis will become part of the permanent collection of Oregon State University libraries. My signature below authorizes release of my thesis to any reader upon request.

_____

Wesley D. Frey, Author

ACKNOWLEDGEMENTS

First I would like to acknowledge my committee members, Dr. Plant and Dr. Jansen for serving on my committee. Furthermore, I would like to acknowledge Dr. Farsoni for his previous research and for his assistance in accomplishing my research in terms of signal acquisition and digital post processing. By my best estimates the ability to process pulses off-line saved a year in research time and probably prevented some non-trivial dose to myself as well.

I would like to thank Dr. Palmer for always defending my decision to become a radiation health physicist, after my undergraduate career as a nuclear engineer, to his students mainly just Matt Cleveland and Nathan Barnett.

On a personal and professional level I cannot thank my advisor Dr. Hamby enough. There were times of personal difficulty where I was given time and space to work things out on my own when professional work was generously allowed to take a backseat. There were also times where the data looked far less than ideal and I began to doubt the validity of my work. It was invaluable to have an advisor who believed in my work, at times, more than I did. Finally, I am grateful for the chance to teach at the university level. Perhaps this one experience at Oregon State University will have the longest lasting effect on my career.

Of course I have to thank my friends and fellow graduate students who provided professional feedback, comic relief, and most importantly a safe place for me talk about my “terrible life decision” to pursue a doctorate.

Lastly I would like to thank my family for their love and support.

TABLE OF CONTENTS

TABLE OF CONTENTS (Continued)

Page

TABLE OF CONTENTS (Continued)

Page

TABLE OF CONTENTS (Continued)

Page

LIST OF FIGURES

LIST OF FIGURES (Continued)

Figure Page

LIST OF TABLES

DEDICATION

This work is dedicated to the memory of my best friend Marcos Rodarte. I am saddened by the fact that I will never get to sarcastically ask you to “get Dr. Wes another beer” on one of our infamous camping trips. I have had many good friends in my life, but only one I ever really thought of as my brother.

Use of BC-523a Liquid Scintillator for Simultaneous Neutron Spectroscopy and Gamma Counting with the Implementation of a Neutron History Reconstruction Algorithm

By
Wesley Frey
Department of Nuclear Engineering and Radiation Health Physics
Oregon State University

1. Introduction

1.1 Overview

Real-time, high efficiency neutron spectroscopy has, historically, been a persistent challenge in the field of radiation detection and, for the most part, has gone unsolved. The most promising method to resolve this challenge, is the boron-capture technique. Detectors that utilize this method possess an unusual property that allows them to be used for estimation of initial neutron energy over a large range of incident energies. As a non-thermal neutron enters the detector volume, the neutron collides with hydrogen atoms in the scintillation material, producing recoil protons. These protons deposit energy in the detector volume producing a scintillation light pulse. The neutron continues to generate recoil protons as it thermalizes inside the detector. The time required for a fast neutron to thermalize is very short, therefore the scintillation pulse resulting from all of the recoil protons will appear as a single prompt pulse. Once the neutron is thermalized, it is likely to be absorbed by a ^{10}B atom in the scintillator. When this occurs, a prompt alpha particle and ^{7}Li nucleus are released following the de-excitation of the ^{11}B compound nucleus. This reaction results in a characteristic second scintillation peak, the delayed boron-capture pulse. If the delayed boron-capture pulse is observed, then the total light output of all the recoil protons is proportional to the initial kinetic energy of the incident neutron. This

property is ideal for a real-time neutron spectroscopy system. Unless an incident neutron leaves the detector and is then scattered back into the active volume, the only way a boron-capture peak can be observed is if the neutron loses all of its kinetic energy inside the detector, as the fast absorption cross section for boron is near trivial.

Although the boron-capture method has existed for over 50 years, there are currently no commercially available systems that are application ready (e.g. mixed field dosimetry and plutonium detection). The two most significant problems with this method are that the recoil proton light response is non-linear and the amount of analog circuitry required to process the pulses is prohibitive. This research is intended to resolve these two problems.

1.2 Goals and Objectives

The overall objective of this research is to develop a prototypic detection system, using extensive post-processing techniques, which will be capable of simultaneous neutron and gamma-ray spectroscopy. This research builds upon previous work by a number of scientists (Aoyama 1993, Klein 2002, Marrone 2002, Jastanish 2004, Britvich 2005, and D'Mellow 2007). This research, however, is distinct for two reasons:

1) this is the first published attempt to correct for the non-linearity in recoil proton light response for the total prompt scintillation pulse; and
2) this is the first time purely digital techniques are used to process the signal without the use of an analog trigger to recognize the boron capture signal pulse.

1.3 Applications

Although the need for improvement in current passive portal monitor systems is a pressing concern, the BC-523a (5% by weight 90% enriched ^{10}B suspended in a liquid scintillation solution) detection system has several foreseeable applications. A number of active detection systems are under development (Flaska 2007, Jordan 2007, and Slaughter 2007) that use a pulse of fast neutrons to detect both ^{235}U and ^{239}Pu. In theory, when a pulse of high energy neutrons is directed into cargo, the fast neutrons quickly thermalize, and become absorbed. The rate at which these fast neutrons thermalize is the quantity of interest. In the event that a fissile material is present, the time it takes for the neutron population to thermalize is much longer; once the fast neutrons from the neutron generator are thermalized, they will induce fissions in the fissile material and produce a new population of fast neutrons that will in turn be thermalized in the cargo. In short, as the thermalization time increases, so does the chance that the cargo contains fissile material. Such a detection system would require a highly efficient neutron detector that can accurately measure neutrons and evaluate their energies. A BC-523a detector could be a suitable detector for this application.

The BC-523a detection system also could be used as a dosimeter for mixed gamma and neutron fields. If both the gamma and neutron spectra were to be measured accurately, a simple computer program could be used to relate these spectra to full-body dose via ICRP flux-to-dose conversion factors (Czirr 2002).

The final potential use of this system stems from the increasing cost and increasingly wide spread use of ^{3}He tubes. Helium-3 tubes are used primarily for high efficiency thermal neutron detection. The most common applications for thermal

neutron detection are non-destructive assay of special nuclear material and portal monitors. Due to its extremely limited natural occurrence and the escalating use of ^{3}He portal monitors, it is possible that ^{3}He tubes will become prohibitively expensive, making an alternative a significant advancement. Plastic scintillators have not been used as an alternative thus far because they have poor gamma-ray and neutron discrimination properties if only a small amount of energy is deposited in the detector (small pulse amplitude). The use of lead shielding to filter out the gamma-ray component of a mixed radiation field would likely make any system extremely heavy. However, if a method can be developed to discern whether a low-energy pulse is a neutron or a gamma-ray, the BC-523a system could prove to be a viable alternative to the ^{3}He tube. Such a system would have the advantage of being constructed from relatively inexpensive material, as well as having neutron spectroscopy capabilities over a wide energy range.

2. Review of Literature

2.1 History of Neutron Spectroscopy

The history of neutron detection begins with the discovery of the neutron itself by Chadwick in 1932. The discovery of the neutron posed a difficult problem to scientists of the time. Namely, how do you detect a particle that has no charge? Chadwick's solution was to measure the charge created by hydrogen atoms that had been scattered by incident fast neutrons. Chadwick was able to infer the existence of the neutron by detecting the ionization created by secondary particles and, in fact, this remains the primary basis for neutron detection.

As the field of neutron detection and nuclear engineering expanded over time, the need for neutron spectroscopy grew. Methods of neutron spectroscopy can be divided into six distinct groups (Brooks 2002).

2.1.1 Neutron Scattering

The neutron scattering method was pioneered by Chadwick. This type of detector measures the recoil energy of an atom scattered by a fast neutron. Typically, these detectors are filled with hydrogen gas. As the recoiled hydrogen moves through the hydrogen gas it causes secondary ionizations in the gas, which are then collected via some applied bias voltage (Ferguson 1958 and Johnson 1958). While these detectors provide accurate spectral information, they are inefficient and are insensitive to thermal neutrons.

2.1.2 Ion Chambers

The measurement of charged particles released when a neutron is absorbed in an atom can also be used to provide spectral information. If the energy released by such a reaction is known, then when a reaction takes place, any energy measured in excess of this baseline energy must be attributed to the incident kinetic energy of the neutron upon absorption (Batchelor 1958). The ubiquitous ^{3}He detector, operates using this principle. While these detectors provide very high energy resolution, they are very inefficient due to the low probability of the fast neutron absorption reaction in ^{3}He.

2.1.3 Time-of-flight

Time-of-flight methods may also be used to calculate the velocity of a neutron, which is directly related to its energy. This method typically works by taking advantage of the fact that most neutron emitters also emit gamma-rays, simultaneously. A fast gamma-ray detector is placed very close to the source and a coincidence gate is set up to detect the near simultaneous response from a neutron sensitive detector some distance away. If two pulses are measured, the time difference between these measurements can be used to determine the neutron's velocity and energy. The primary drawback to this method is that the source location must be known precisely in order to calculate neutron speed (Neiler 1958).

2.1.4 Threshold Reactions

Similar to the second method is the threshold reaction method, where some threshold neutron energy is needed for a neutron absorption reaction to take place. Once the reaction has occurred, a gamma-ray of specific energy is released and is measured to confirm the neutron reaction. The primary drawback to this method is that no information concerning the neutron population below the threshold energy can be derived (Brooks 2002).

2.1.5 Spectral Unfolding

Spectral information can be estimated by unfolding a set of measurements from a series of detectors with different thicknesses of moderating material surrounding them. The unfolding is accomplished by using a response matrix based on average detector response for a given neutron energy. The most common example of this style of detector is the Bonner sphere detection system. The most significant drawback to this detection system is that it does not provide real-time data. Several measurements are required before the unfolding process can take place (Bramblett 1960).

2.1.6 Neutron Thermalization Time

The final method can be used to measure the energy of a short burst of neutrons. As a burst of neutrons moves through a medium it becomes thermalized. If the physical properties of the medium are known precisely, the time required for the neutrons to become thermalized (and detected by a thermal neutron detector) can be used to calculate the incident neutron energy. This technique is only useful if the

physical properties of the thermalizing medium are known (Flaska 2007, Jordan 2007, and Slaughter 2007).

2.1.7 Recent Trends in Neutron Spectroscopy

The majority of neutron spectroscopy methods were developed in the two decades following Chadwick's discovery. These methods include hydrogen proportional counters, recoil telescopes, ^{3}He proportional counters, time-of-flight methods, lithium iodide scintillation crystals, threshold reaction methods, and capture-gated spectrometers. As the field moved into the 1960's and 1970's, the introduction of computers began to advance neutron spectroscopy to its current state. The most notable spectroscopy method to come from this time was the Bonner sphere method. For this method computer codes were used to construct a response matrix for a given detector. As the field moved into the 1980's and 1990's the role of the computer (and computational power) continued to push the evolution of neutron spectroscopy methods. Work during this time focused mainly on the use of Monte Carlo codes to simulate detector response and to optimize detector geometry in order to maximize efficiency. Currently, the field is undergoing a significant transition from analog signal processing to digital signal processing. This advance has only recently become feasible due to the recent advances in computer processing power and memory capacity. Digital processing should be more flexible, stable, and cheaper than current analog techniques. Complex real-time data correction and data manipulation techniques may also be possible with all-digital processing.

Gamma-ray spectroscopy has long had its “ideal” detector in the form of the high purity germanium detector (HPGe). The HPGe has outstanding energy resolution that is capable of identifying gamma-ray emitting nuclides. While the HPGe does not possess the intrinsic efficiency of other gamma-ray sensitive detection systems, it remains the overwhelming choice for most gamma-ray spectroscopy applications. In contrast, neutron detectors capable of neutron spectroscopy remain application specific. There exists no high-efficiency neutron detector capable of real-time, high energy resolution spectroscopy. The origins of this problem are in the physics of neutron interactions with matter. While gamma-ray interactions (photoelectric effect, Compton scattering, and pair production) produce large numbers of ion pairs (or light photons for scintillation detectors), in turn resulting in more precise energy resolution, fast neutron interactions tend to produce relatively few ion pairs, resulting in poor energy resolution. Furthermore, neutron absorption cross sections tend to increase rapidly as neutron energy decreases. This results in relatively few neutrons being absorbed at high energy making several of the six neutron spectroscopy methods very inefficient. Therefore, when neutron spectroscopy is required, one must make a tradeoff between resolution, efficiency, real-time operation, and the size of the system. Often, one of these properties will come at the expense of another, making a compromise essentially mandatory.

2.2 Fundamental Interactions

2.2.1 Gamma-Ray Interactions

Gamma-ray interactions are generally considered to be described by five mechanisms: photo-electric effect, Compton scattering, pair production, Rayleigh scattering, and photodisintegration. The latter two mechanisms, however, are not particularly relevant when examining gamma-ray response in a radiation detector.

In the photoelectric effect a gamma-ray interacts with an inner-shell bound electron of the target atom. The electron is ejected from the atom with an energy equal to the incident gamma-ray energy minus the binding energy of the electron. If the energy of the incident gamma-ray is less than the binding energy of the electron, the reaction will not take place; it is in this way that the reaction is considered a quantized reaction. The photoelectric effect is dominant at lower gamma-ray energies (<100 keV) and for target atoms with a high effective Z:

$$\tau \propto Z^4/(h\upsilon)^3, \tag{1}$$

where τ is the photo electric interaction coefficient.

The Compton effect, or Compton scattering, takes place when a gamma-ray collides with a loosely bound electron. Unlike the photoelectric effect, the incident gamma-ray is not completely absorbed, rather it is scattered to a lower energy and the target electron is recoiled. The energy of the recoiled electron is equal to the incident gamma-ray energy minus the energy of the scattered gamma-ray. The Compton effect is dominant at mid gamma-ray energies (>100 keV and <2 MeV) with the coefficient of interaction, σ , given by:

$$\sigma \propto Z/h\upsilon. \tag{2}$$

During pair production, a high energy gamma-ray passes close to the nucleus of an atom and interacts with its strong electromagnetic field. In this interaction the incident gamma-ray is completely transformed into an electron-positron pair. Due to conservation of mass and energy, the minimum energy required for a gamma-ray to undergo pair production is the mass of the positron-electron pair or 1.022 MeV. This effect will dominate at high gamma-ray energies (>2 MeV) with the coefficient of interaction, κ, given by:

$$\kappa \propto Z^2 (h\upsilon - 1.022). \tag{3}$$

The total gamma-ray interaction probability coefficient, μ, is given by:

$$\mu = \tau + \sigma + \kappa. \tag{4}$$

This total interaction probability coefficient, obeys first order kinetics. Thus, the change in uncollided gamma-ray flux, with respect to distance traveled through the shielding material (dx), is equal to the negative flux multiplied by the gamma-ray removal coefficient or μ. In differential form this equality appears as:

$$\frac{d\phi}{dx} = -\mu\phi, \tag{5}$$

where x is the thickness of the shielding material or the path length through a detector. It follows that the probability of a given photon, undergo an interaction between 0 and x, is

$$P = 1 - e^{-\mu x}. \tag{6}$$

2.2.2 Neutron Interactions

Neutron interactions are generally divided, by their energy into two categories: fast neutron collisions and thermal neutron absorption. The change in fast neutron

flux, with respect to the distance traveled through the shielding material (dr), is equal to the negative flux multiplied by the neutron total cross section:

$$d\phi = -\phi\Sigma_{rm}dr\,. \tag{7}$$

This removal coefficient Σ_{rm} (macroscopic removal cross section) represents the probability that the neutron will undergo any interaction that will reduce its kinetic energy enough to remove it from the fast group. For a point neutron source the total fast flux, at distance r, will be:

$$\phi(r) = \phi_o e^{-\Sigma_{rm}r}\ , \tag{8}$$

where r is the distance from the point source including the shielding or detector thickness and ϕ_o is the initial flux. For example, a 2 MeV neutron source incident pure beryllium would have a macroscopic cross section of 0.132 cm^{-1} (Lamarsh 2002). Therefore, the fraction of neutrons (total fast flux) passing through 100 cm of beryllium without an interaction would be equal to:

$$e^{-(0.132cm^{-1})(100cm)} = 1.85*10^{-6}\,. \tag{9}$$

Given that only 1.85 neutrons out of one million will be able to pass through the beryllium without a single interaction, it is clear that fast neutrons interact easily with beryllium, reducing their energies. However, this is somewhat misleading because each collision with beryllium produces only a small energy loss to the neutron. Assuming only potential scattering will take place, this energy loss is given by:

$$\Delta E = 0.5*(1-\alpha)*E_o\,, \tag{10}$$

where E_o is the initial energy of the neutron and α is the collision parameter equal to

$$\alpha = \left(\frac{A-1}{A+1} \right)^2 , \tag{11}$$

where A is the atomic mass of the target nucleus. In the case of beryllium, a neutron would be required to undergo 69 collisions to reduce its energy from 2 MeV to 1 eV. An ideal moderator, therefore, would be low in atomic mass to maximize energy transfer per collision, as well as to have a large macroscopic cross section to increase the probability of interaction. In fact, moderating power is a quantity defined as "mean lethargy gain per collision" multiplied by macroscopic scattering cross section, where mean lethargy gain per collision is defined as:

$$\xi = 1 + \frac{\alpha}{1-\alpha} \ln \alpha . \tag{12}$$

Once a neutron has been fully moderated, it is at thermal equilibrium with the surrounding environment. By definition it can no longer impart significant kinetic energy to surrounding atoms. At this point the neutron can only be removed by a capture reaction or leakage, which is also characterized by a cross section and first order kinetics. These cross sections range widely from a few barns in hydrogen to several thousand barns in cadmium. The ideal material to stop or detect thermal neutrons would have a high absorption cross section. Typically, when a thermal neutron is absorbed in a target atom, the atom is raised to an excited state. From this excited state the atom will likely rapidly emit subsequent radiation to become stable. It is this secondary prompt radiation that can be detected in order to infer the presence of thermal neutrons.

2.2.3 Cosmic Muon Interactions

Cosmic muons are the final interaction that must be investigated when looking at modeling the response of a large active volume, low Z detector. The particles are often referred to as super massive electrons as they have the same charge as an electron, but with a mass 209 times that of an electron. Given that these particles lose kinetic energy via collisions with much less massive orbital electrons, they lose energy gradually and their trajectory is not easily deviated. Cosmic muon energies span an enormous range from a few eV up to 10^{10} GeV, but most cosmic muons have energies below 10 GeV. Cosmic muons interact continuously with the atmosphere until they reach the surface of the earth with an average energy of 3 GeV. At this energy the muons have a stopping power of 2 MeV g^{-1} cm^{-2}. It is this value that can be used to estimate energy deposited in a shield or a detector as a function of the path length through a material (Gilboy 2007). These cosmic muons can interfere with detector operation by causing false positive signals, which are identified as either gamma-rays or neutrons. The false positive rate will be relatively constant as the muon flux incident on the Earth's surface is relatively constant (though it does vary somewhat with latitude). The amplitude of these false positives will be dependent on the muon's path length through the detector.

2.3 The Boron-Gated Neutron (BGN) Capture Method

The ideal neutron spectrometer, to be used in a portal monitor, would have good energy resolution and high efficiency for thermal to fast neutron energies. Furthermore, such a detector would have excellent gamma-ray discrimination and would yield the neutron spectrum in real time. Current methods of neutron

spectroscopy, however, are far from ideal. Bonner-sphere results can be accurate if a sufficiently large number of spheres are used; however, such systems are large and can not provide real-time spectral information. Helium-3 and hydrogen proportional counters provide high resolution, but have very low efficiency. Typically, several detectors must be used in tandem to obtain useful working efficiencies, making such systems large and expensive.

An alternative neutron spectral measurement system could use the boron-capture gated method. Liquid scintillation materials appear to be the most promising for such a detector, as they exhibit superior gamma-ray discrimination properties and they have a higher hydrogen-to-carbon ratio than their solid counterparts. A large hydrogen-to-carbon ratio is important because neutrons colliding with carbon will not result in a measurable scintillation pulse. One such scintillation material is BC-523a which has an atomic composition in atoms per cubic centimeter (as reported by the manufacturer Saint Gobain) of 4.98e22 hydrogen, 2.86e22 carbon, 8.11e21 oxygen, 2.43e21 boron-10, and 2.7e20 boron-11; with a total physical density of 0.916 g/cc. Previous efforts have focused on this method (Aoyama 1993, Colonna 1998, Lee 1998, Jastaniah 2003, Britvich 2004) because of its characteristic gamma-ray discrimination and high intrinsic efficiency (10% for neutrons in the low MeV range). Similar work has been completed using a liquid scintillation system doped with ^{6}Li and yielded similar results (Aleksan 1988 and Bertin 1993).

Boron-capture gated neutron (BGN) detectors possess an unusual property that allows them to be used for estimation of initial neutron energy over a large range of incident energies. As a non-thermal neutron enters the detector volume, the neutron

collides with hydrogen atoms in the scintillation material producing recoil protons. These protons deposit energy in the detector volume producing a scintillation light pulse. The neutron continues to generate recoil protons as it thermalizes inside the detector. Total light output of all the recoil protons is proportional to the initial kinetic energy of the incident neutron. The time required for a fast neutron to nearly thermalize is less than the resolving time of a typical organic scintillator (on the order of a few nanoseconds), therefore the scintillation pulse resulting from all of the recoil protons will appear as a single pulse. Once the neutron is thermalized, it is likely to be absorbed by a ^{10}B atom in the BC-523a. When this occurs, a prompt alpha particle (~1.5 MeV) is released following the de-excitation of the ^{11}B compound nucleus. This reaction results in a characteristic second scintillation peak. The time required for the neutron to be captured by ^{10}B is much longer than the time required for thermalization. The result, therefore, is two distinct signal pulses that are easily distinguishable; the fast recoil proton pulse, followed by the delayed boron-capture pulse (Fig.1).

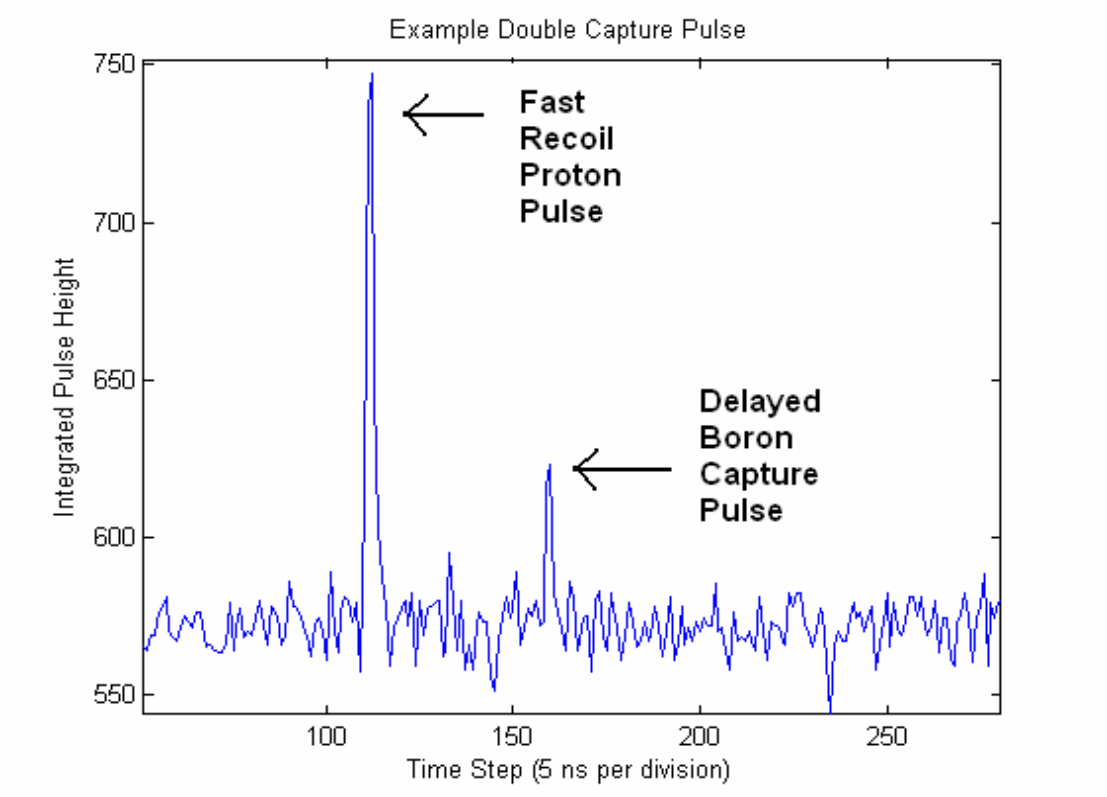

Fig. 1. Example double capture pulse.

Unless an incident neutron leaves the detector and is then scattered back into the active volume, the only way a boron-capture peak can be observed is if the neutron loses almost all of its kinetic energy inside the detector. Detection electronics can be arranged to identify the characteristic boron-capture peak. The system is gated in the time domain (either with analog or digital techniques), so that the first scintillation pulse, produced by the recoil protons, is counted only if the second peak is observed. This detection technique results in recoil proton signals proportional in amplitude to the incident energy of the neutron.

2.3.1 Current Limitations of the BGN Method

At first glance, the BGN system appears to be an ideal neutron spectrometer. However, one significant complication exists due to the fact that scintillation light output is not linearly proportional to recoil proton energy. Light response in BC-523a is proportional to E^X, where E is the recoil proton energy and X is some value between 1 and 2 (Aoyama 1993). The problem, therefore, is that neutrons transferring the majority of their kinetic energy in relatively few collisions will generate scintillation pulses of higher amplitude than the same neutron transferring energy over a larger number of collisions, thus appearing to be of higher initial energy. Current boron-capture gated spectra for monoenergetic neutrons are very broad and shifted to higher corresponding neutron energies (Aoyama 1993, Britvich 2005) because of this phenomenon.

2.3.2 Current Research into the BGN Method

Previous research efforts have focused on the validation of the MCNP and GEANT codes that simulate the light output of specific organic scintillation materials as a function of incident neutron energy (Kamykowski 1992, Aoyama 1993, and Patronis 2007). Other research efforts have focused on experimentally determining the recoil proton response function from fast monoenergetic fusion neutron sources (Lee 1997). Recently there has been interest in using continuous-energy neutron sources (^{252}Cf) in order to measure recoil proton scintillation response for incident neutrons with energies below 1 MeV (Colonna 1998). Results are encouraging given that these lower energy neutrons (and resulting recoil protons) generate stronger

scintillations than previously thought, meaning that BGN detectors may provide neutron spectral information down to, and maybe even below, 0.1 MeV.

Little research has focused on real-time correction algorithms that compensate for the characteristic overestimation of the neutron incident energy, or the poor intrinsic resolution associated with the BGN spectroscopy method. A few research groups (Czirr 1994 and Abdurashitove 2002) have constructed neutron spectroscopy systems that theoretically account for this non-linearity. Their efforts have focused on building plastic scintillation detectors with multiple, thin, optically decoupled layers. The idea is that these layers are so thin that it is likely that only one neutron/proton collision will take place per layer. If the light response function for protons is known, then the energy deposited in the detector can be calculated because the non-linearity in light response can be corrected for one neutron/proton collision at a time. If it is known (via neutron capture reaction) that the neutron has lost all of its energy in the detector, then the neutron's incident energy can be inferred. The major drawback of this system is that if more than one neutron/proton collision takes place in a layer, the system will be unaware and will output an incorrect neutron energy.

2.4 Scintillation Detector Principles

2.4.1 Scintillation Theory

All organic liquid scintillators emit light upon the absorption of ionizing radiation by three distinct mechanisms: fluorescence, phosphorescence, and delayed fluorescence. Fluorescence is the process typically considered as prompt light emission. When energy is deposited in a system, via an interaction with ionizing

radiation, it can be transferred to pi-electrons. These electrons are then excited to a number of singlet states (electron spin remains zero). These excitation states are unstable, consequently the electrons quickly decay back down to the ground state by the emission of a photon (typically in the ultraviolet range). The rate at which these excited electrons decay back to the ground state can be modeled by first order kinetics,

$$I = I_o \exp(-t/\tau), \tag{13}$$

where I is the instantaneous emission intensity, I_o is the initial emission intensity , and τ is the fluorescence decay time. In the case of BC-523a this decay constant is 3.7 ns. This scintillation mechanism is dominant in the BC-523a material for gamma ray interactions.

Phosphorescence begins the same as fluorescence except instead of the electron being excited to the singlet state, the electron changes its spin (to spin 1) and is excited into a triplet state. This transition from singlet to triplet state is known as inter-state crossing. These triplet states are always at a lower energy level than their corresponding singlet states. These excited electrons can also decay back down to the ground state by the emission of a photon. The rate of this decay can be described by equation 13 except the decay time is significantly longer, on the order of milliseconds. For liquid scintillators the fraction of energy deposited by radiation that is converted into phosphorescence photons is nearly trivial, and can be ignored.

Delayed fluorescence is similar to phosphorescence in that an electron is excited to a triplet state via inter-state crossing. These electrons may return to a singlet state if some additional energy is imparted to the electron. Typically, this process occurs when two electrons are excited to a triplet state. These excited

electrons interact and one electron is returned to the ground state while the other is returned to a singlet state, which then decays to the ground state. Both electrons produce a photon; however, it is the electron returning to the singlet state that is responsible for the delayed fluorescence. The fraction of radiation energy deposited in the detector that is converted to delayed fluorescence photons is dependent on the density of electrons excited to triplet states. This density is dependent on the linear energy transfer (LET) of the incident radiation (D'Mellow 2007).

Gamma rays and the fast electrons they produce (via photoelectric effect, Compton scattering, and pair production) have a relatively low LET and as a result will have a relatively small fraction of delayed fluorescence photons produced per unit of energy deposited in the system. Conversely, neutrons and the fast protons they produce have a relatively high LET and as a result will produce a much larger fraction of delayed fluorescence-photons. The final result of these physical mechanisms of scintillation is that gamma-ray scintillation pulses decay noticeably faster than neutron-scintillation pulses. A number of techniques, for using this difference in pulse shape to discriminate pulses are explored later in this paper.

Given that different particle types of the same energy produce different scintillation pulse amplitudes, a unit must be used to normalize the amplitude of the resulting scintillation pulse as a function of particle energy. This unit is known as keV electron equivalent (keVee). Essentially, this unit describes the amplitude of the scintillation pulse if that amount of energy were deposited in the system by fast electrons. For example, if a 100 keV gamma-ray deposits all of its energy in a scintillator, the resulting pulse amplitude would be 100 keVee. However, if a 100 keV

proton deposits all of its energy in the same scintillator, the resulting pulse amplitude would not be equal to 100 keVee, it would be some value less than 100 keVee (depending on scintillator type) because protons are less efficient at producing scintillation light than fast electrons.

2.4.2 Scintillation Pulse-Shape Analysis

Any detection system intended to detect more than one type of radiation must be able to discriminate between these various types. A pulse-shape discrimination technique will allow the BC-523a system to differentiate recoil protons (neutron interactions) from recoil electrons (gamma ray interactions). One reason for the selection of BC-523a is because of its excellent pulse shape discrimination (PSD) capabilities (Jastaniah 2003).

The basis for all pulse shape discrimination techniques in organic scintillation (e.g. BC-523a) is the fraction of fluorescence and delayed fluorescence light produced by a given radiation type. That is to say, different radiation types will produce differently shaped pulse profiles in terms of current from the anode of the PMT vs. time. Various pulse-shape discrimination techniques characterize this difference in pulse shape in unique ways, although all of the techniques provide theoretically very similar separation fidelity (Jastaniah 2003).

There are two widely accepted methodologies for analog PSD, including “10%/90% pulse rise time” or the “time-over-threshold” method. The 10%/90% pulse rise time method requires measuring the time it takes for an incoming signal pulse to increase from 10% of its maximum voltage amplitude to 90% of its maximum

amplitude (from the output of an integrating preamplifier). Due to their difference in rise times/LET's, electron signal pulses will have a much shorter 10%/90% rise time than protons.

The time-over-threshold method is similar to the 10%/90% method. This method produces the time at which a pulse exceeds some threshold current (measured from the anode of the photomultiplier). Once again, due to the difference in rise times/LET's, fast electron signal pulses will have a small time-over-threshold relative to recoil protons. Both of these methods are well established, however, they are more applicable to analog circuitry and would likely not be the most suitable for digital signal processing.

Pulse-shape discrimination techniques have been developed recently that are simpler to implement in the digital environment. The double charge integration and pulse gradient analysis methods (D'Mellow 2007) take advantage of the difference in fall times of the gamma/neutron pulses. The double charge integration pulse shape discrimination technique integrates the charge of a given pulse from the beginning of the pulse out to two distinct integration times. The first integration time is selected to correspond to 2-4 times the magnitude of the fluorescence decay time (fast charge component). While the second integration time is chosen to be 2-4 times the magnitude of the delayed-fluorescence decay time (total charge component). The total-to-fast charge ratio of these two integrals is then taken, to be used as a quantity to discriminate gamma-rays from neutrons. Gamma-ray scintillation pulses decay more quickly than neutron scintillation pulses and therefore have a smaller total-to-fast charge ratio than neutrons.

The pulse gradient analysis method uses the gradient of the decaying side of the scintillation pulse. This gradient is based on two points; the peak of the pulse and some point down range where the difference in the height of a gamma pulse and neutron pulse is most pronounced. This gradient is then normalized to the pulse amplitude. Once again, due to the difference in pulse decay rates, gamma rays will have a smaller gradient-to-pulse-height ratio than neutrons. This technique is essentially identical to the decay time fitting method where the fluorescence and delayed- fluorescence decay times are calculated.

Due to recent increases in waveform digitizer sampling speeds, and given the fact that BC-523a's prompt scintillation decay time is on the order of the average time between fast neutron collisions in BC-523a, an altogether new discrimination technique may be possible (Reeder 1999). As a fast neutron enters the active volume of the BC-523a detector it begins to generate recoiled protons, which generate the prompt scintillation pulse. If the fast waveform digitizer is relatively slow, all of the individual recoil proton pulses will appear as one prompt pulse. However, if the wave form digitizer is sufficiently fast a "saw tooth" pattern will be seen at the peak of the prompt scintillation pulse, where each "tooth" represents the light produced from one recoil proton. If each individual "tooth" could be resolved, then the non-linearity associated with the recoil proton's light response could be corrected fairly easily. However, if the fast neutron collisions take place more rapidly than BC-523a's prompt scintillation's decay time, then the individual proton scintillation pulses cannot be resolved. In fact, this scenario is likely, given that the time between fast neutron collisions is about 1 ns while the prompt scintillation decay time for BC-523a is 3.7

ns. However, the prompt scintillation peak from fast electrons (created by a gamma-ray) is well defined, while the peak of fast neutrons will be "saw toothed." Even though not all of the individual proton scintillation pulses can be resolved, this general saw tooth feature is indicative of a neutron interaction and could be used to identify neutrons with very high fidelity.

2.5 The Neutron Collision History Reconstruction Algorithm

2.5.1 Technical Issue

The most significant technical issue resulting from the use of any boron-containing organic scintillation material for neutron spectroscopy is the non-linear light output from recoil proton energy depositions. This light output function is close to $E^{3/2}$ (where E is the energy of the recoil proton) for organic scintillation materials. However, the accuracy of any correction algorithm is highly dependent on detailed knowledge of the recoil-proton response function for the specific organic scintillator in use.

For the discussion that follows, it is assumed that the response function is $E^{3/2}$ for all proton energies. When a neutron with significant kinetic energy (tens of keV to a few MeV) enters the detector, it will undergo a number of scattering events before it is slowed to an energy where boron capture is likely. Neutrons can impart between 0 and 100% of their incident kinetic energy to a hydrogen atom at each collision. Because the energy transfer probability is independent of energy, the average energy lost by a neutron per collision is one-half its incident energy. One characteristic of the $E^{3/2}$ response function is that a single, higher-energy recoil proton will be weighted

more heavily, in terms of scintillation light output, than multiple lower-energy protons having the same total energy. For example, a 2 MeV recoil proton will always produce a higher light output than the sum of two 1 MeV recoil protons. The result of this relationship is that fast neutrons that require fewer collisions, on average, to become thermalized, will produce a scintillation light pulse of higher amplitude than expected relative to a linear response system (Aoyama 1993).

2.5.2 Recoil Proton Response

Before a correction algorithm can be applied to the raw data from the BGN detector, the recoil proton response of BC-523a must be well defined. Previous investigations have been carried out to examine proton response in organic scintillators (Aoyama 1993, Lee 1997, Colonna 1998, Britvich 2005). Early research in the mid-1990's focused on using high energy monoenergetic neutrons produced by various fusion reactions (Aoyama 1993, Lee 1997). These experiments mapped out the recoil proton response of organic scintillators in the energy range of 1 to 14 MeV. More recently there has been increased interest in using continuous energy neutron sources to measure recoil-proton response (Colonna 1998, Britvich 2005). These later experiments have shown the detector response at lower neutron energies (<0.1 MeV) is higher than expected and well above the detection threshold. Colonna (1998) used a ^{252}Cf source and BC-510 (non-borated liquid) for detection, while Britvich (2005) used a PuBe source and SC-331 (boron-doped plastic) to demonstrate recoil proton response.

2.5.3 Other Technical Issues

2.5.3.1 Non-Hydrogen Collisions

To this point, we have assumed that the scintillation material is pure hydrogen. Although hydrogen has the highest average scattering cross section and atomic fraction of the constituents in BC-523a (hydrogen, carbon, oxygen, and boron), the reconstruction algorithm will propagate a systematic error if no consideration is given to these other atoms. The carbon, oxygen, and boron "impurities" in the scintillation material will be accounted for in the neutron history reconstruction algorithm by estimating the likelihood of a non-hydrogen collision as a function of neutron energy. Because the kinetic energy transferred to these heavier atoms will be relatively small and scintillation light output falls off with increasing charge on the recoil atom, the scintillation pulses from these recoil atoms is thought to be insignificant. Therefore, the revised correction method will only take into account neutron energy loss (and not light production) from the carbon, oxygen, and boron collisions.

2.5.3.2 Inelastic Scatter Photons

At higher incident neutron energies (>5 MeV) carbon, oxygen, and boron inelastic scatter will become significant. If the resulting gamma ray is absorbed in the detector, a gamma ray discrimination technique can be used to discard the entire neutron history. However, it is also possible that the inelastic gamma-ray will leave the detector. This will result in an underestimation of the incident neutron energy. To quantify, and possibly correct for this effect, particle transport simulations must be carried out to predict, as a function of incident neutron energy, the fraction of energy

leaving the detector volume as gamma-rays from inelastic scattering of neutrons. The results of these simulations then can be used to modify the neutron history algorithm to improve accuracy at higher neutron energies.

2.5.3.3 Intrinsic Neutron Absorption Efficiency

It is important to remember when modeling detector response with computational methods that these responses represent an ideal detector response. This ideal detector response will differ from the actual detector response, in terms of response as a function of incident neutron energy. This difference between detector response and flux can be corrected if the detector's neutron response function is known.

2.5.3.4 482 keV Capture Photon Effect

An effect that causes the actual detector response to differ from the theoretical detector response is the emission of the 482 keV photon (94% of the time) when a thermal neutron is absorbed in a ^{10}B atom. There is a small probability that this photon will be absorbed in the detector, causing an overlapping pulse from a neutron absorption pulse and from the 482 keV photon (which will likely be Compton scattered). It is unclear if this pulse can be properly identified as a combination of heavy ions and fast electrons. It is therefore important to understand the extent of the 482 keV photon effect so that proper corrective action can be taken to prevent significant loss of efficiency and to minimize false positives/negatives.

2.6 Particle Misidentification Problems

Given that no particle identification process is 100% accurate, one must account for, or at least discuss, the possible false positives and false negatives of any system. The identification software for the BC-523a detector has six true positive outcomes; cosmic muon, high energy gamma-ray, fast neutron with thermal neutron capture, fast neutron without capture, thermal neutron capture, and 60 keVee from a muon, gamma-ray, or fast neutron (which will all resemble the pulse generated by a thermal neutron capture in boron). These true positives, along with the associated false positives, are illustrated in Fig. 2.

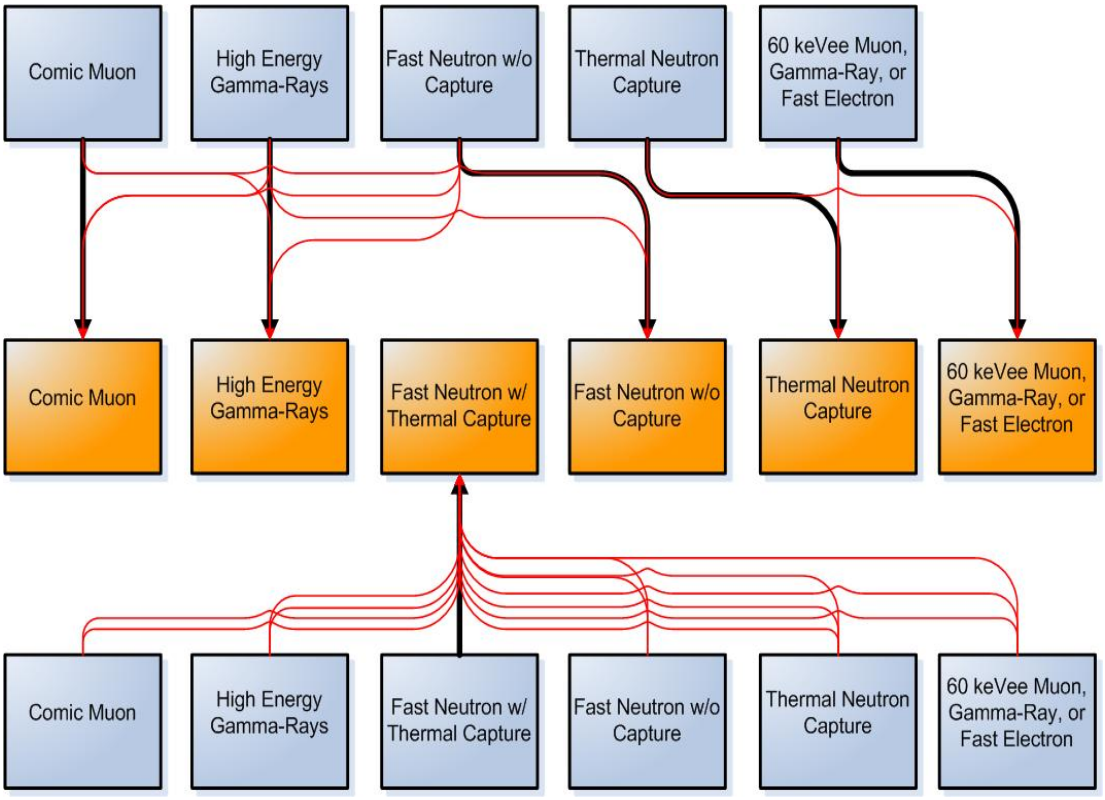

Fig. 2. Particle misidentification diagram.

These true events can be seen above in orange while the event recorded by the detector is depicted in blue. The events are broken into two categories: single events

listed on the top blue row and double events listed on the bottom blue row. The double events arise from the fact that, in order to perform neutron spectroscopy with the BC-523a detector, a double pulse is required to identify a fast neutron that was thermalized in the detector (a prompt fast neutron pulse and a delayed 60 keVee pulse resulting from the thermal capture of a neutron in ^{10}B). The incidence of false positives and false negatives for the single events will be a function of how well the pulse shape discrimination algorithm characterizes the shape of each pulse. The quality of pulse-shape discrimination will also be a function of waveform digitizer speed and of pulse amplitude. As the digitizer sampling speed increases, the recorded shape of the pulse will more closely match the actual pulse-shape. As the magnitude of the pulse increases, the statistical fluctuations will decrease, thus increasing the confidence that the recorded pulse shape closely matches the actual pulse shape.

The incidence of false positives and false negatives for the double events will be a function of, the factors effecting single events and source strength and boron capture gate time (i.e., the length of time the algorithm permits a 60 keVee pulse to be associated with a prompt fast neutron signal). The longer this time, the more efficient the system will be in identifying all true fast neutrons thermalized in the detector. However, if this time is set to be very long, the likelihood that a stray 60 keVee pulse would be associated with a prompt neutron pulse will increase. This increase in gate time will also increase the chance that a neutron entering and leaving the detector will be associated with a 60 keVee thermal neutron capture for a different neutron. Therefore, this gate time must be set to preserve a high fast neutron (that are thermalized in the detector) identification efficiency, but it must be limited to

minimize the rate of false positives and false negatives. The concept of boron capture gate time ties closely to source strength. If the source strength is very large, many 60 keVee pulses and fast neutron pulses will be observed. This in turn will cause an increase in the number of false positives and false negatives. Therefore, the source strength should be taken into account when selecting a boron capture gate time.

3. Materials and Methods

3.1 Implementation of the Neutron History Reconstruction Algorithm

The thermalization of fast neutrons within the detector occurs on a time frame that is too fast (approximately 1 nanosecond between collisions) for individual proton collisions to be resolved, due to the relatively slow prompt scintillation decay time (3.7 nanoseconds for BC-523a). As a result, information regarding individual collision histories is lost. However, the statistics governing those collisions are known. It is therefore possible to predict, on average, the number of collisions (in terms of fractional energy loss) that took place during the thermalization of any given incident neutron. This prediction, however needs to be corrected because a scintillation pulse will be recorded that results in a characteristic overestimation of the incident neutron energy. To negate this systematic, non-linear overestimation, a reconstruction algorithm must be developed to operate on the detector response to correct for an "unknown" collision history. The algorithm would function on the premise that individual neutron histories can be reconstructed, assuming the neutron undergoes an "average" energy transfer during every collision. Therefore, for a sufficiently large group of scintillation pulses, this reconstruction algorithm would mathematically force the signal pulse distribution to be centered about the actual incident neutron energy.

The neutron collision history reconstruction algorithm to be developed in this work will require a two step process, including a "multi-collision" correction and a "within-collision" correction. Three assumptions are required to implement this method. First, every neutron loses, on average, one-half of its energy with every

hydrogen collision. Second, the recoil proton scintillation response is known for BC-523a (Aoyama 1993). And third, the average energy of neutrons that are absorbed by boron is known and relatively constant. Using a customized MCNP model (which measures the time between neutron interactions and the energy at which they undergo these interactions), Aoyama (1993) has determined that, in BC-523a, neutrons are absorbed by ^{10}B at an energy of approximately 10 eV, the vast majority of the time.

The steps, therefore, of a multi-collision correction are as follows:

(1) Scintillation signal pulse is recorded from the BGN detector system;

(2) Neutron history reconstruction begins at the average neutron absorption energy, E_o;

(3) The last neutron collision is simulated. Neutron energy is doubled and a recoil proton of energy E_o is created;

(4) The corresponding scintillation pulse from the recoil proton is calculated using the recoil proton response function (currently assumed to be $E^{3/2}$);

(5) Steps 3 and 4 is repeated, typically several times, and the total scintillation pulse for all simulated recoil protons is tallied; and

(6) This iteration loop stops when the total scintillation pulse for the simulated recoil equals the scintillation pulse measured in step one.

The multi-collision corrected neutron energy is then the energy of the reconstructed neutron (step 3) when the total scintillation pulse for the simulated recoil protons equals the measured scintillation pulse. Although this method appears to be an iterative process for each neutron history, it can be performed only once; since the initial neutron energy is assumed to be constant and the recoil proton response

function is also constant for a given scintillation material, the reconstruction algorithm will be nearly identical for all neutron histories. The only difference between neutrons is that the end-point of the iteration, based on the different scintillation outputs, will vary. The total light output from the simulated recoil protons will be plotted against the corrected incident neutron energy and an empirical fit can be made to the data. The result is a one-step single equation correction of neutron energy.

Once the multi-collision method is applied, a significant improvement is expected in correlating the average detector response with incident neutron energy. However, a constant overestimation in neutron energy is expected to remain across a wide range of incident neutron energies. This is a result of the fact that within a single neutron collision the average energy loss (average recoil proton produced) does not correspond to the average scintillation pulse produced for a single collision. Once again, this is due to the non-linear response function of the scintillation material. Therefore, a second "within-collision" correction must be made so the average corrected detector response will match the actual incident neutron energy. The correction factor is only dependent on the recoil response function of the scintillation material.

The average light output per collision for an $E^{3/2}$ response is given by:

$$\frac{\int E^{3/2} dE}{\int dE}, \tag{14}$$

where the limits of integration are between 0 and E, representing the energy range of possible recoil protons. The integration of Eqn. (14) yields

$$\frac{2}{5}(E)^{3/2}. \tag{15}$$

The average recoil proton will possess an energy of ½ E, such that the scintillation pulse produced will be proportional to,

$$\frac{1}{2}(E)^{3/2}. \tag{16}$$

To obtain the within-collision correction factor, we divide Eqn. (15) by Eqn. (16). For the $E^{3/2}$ response function, the within-collision correction factor is, therefore, 0.8.

A large number of neutron histories will be simulated in a purely hydrogenous material in order determine the expected distribution of a monoenergetic neutron source (assuming an $E^{3/2}$ recoil proton response). This data set will then be processed using the neutron history reconstruction algorithm to demonstrate the potential improvement of the algorithm.

The underlying advantage of this reconstruction technique is that it is computationally inexpensive and, therefore, will be suitable for real-time neutron spectroscopy. If the recoil proton scintillation response function for a given scintillation material is known, the multi-collision and within-collision corrections have only to be determined once. Generally, algorithms that reproduce neutron spectra require solving a response matrix after all the data have been collected. With the development of this neutron history reconstruction algorithm, the data can be corrected in real time.

3.2 Estimation of Error Associated with the Neutron History Reconstruction Algorithm

In order to estimate the error associated with the neutron reconstruction algorithm, a computer simulation will be carried out. This simulation assumes that the scintillation material is infinitely large, purely hydrogenous, and that the recoil proton response function is $E^{1.5}$. Six neutron energies will be simulated by transporting 1000 neutrons of each energy. During this process the neutron will lose between 0 and 100% (the actual fraction will be calculated by the sampling of a random number) of its kinetic energy per collision with hydrogen. The recoil proton response function will then be used to calculate the magnitude of the "virtual" scintillation pulse produced by each neutron. Once the scintillation pulse of all of the neutrons has been recorded, the neutron history reconstruction algorithm will be performed. The result will be a neutron pulse height distribution for each initial neutron energy. The error associated with the algorithm will be estimated by calculating resolution (full width half max divided by the center channel energy) of each of these distributions. It should be noted that this error/theoretical resolution does not take into account the error associated with the natural fluctuation in the number of scintillation photon generated in the detector, any non-linearities in the detector's response, or the error that will result due to interactions with the non-hydrogen constituents of BC-523a.

3.3 Detection System

The BC-523a detection system (Fig. 3) used herein is a departure from the standard analog capture gated neutron spectrometer nuclear instrumentation module (NIM) detection system (Aoyama 1993).

Fig. 3. 12.7 cm diameter by 7.62 cm deep BC-523a detector.

More recent research in the boron-capture gated technique has been conducted using a half analog/half digital system (Jastaniah 2003). The analog portion of their system uses standard NIM's in order to provide a trigger to separate the prompt scintillation pulses that have an associated boron capture pulse from all other pulses in the detector. The digital half of Jastaniah's system begins as the analog signal and trigger enter a waveform digitizer. This system will only digitize neutron pulses that contain spectral information, i.e. the pulses that are triggered. The advantage of their unit is that it is easily modified via an additional input into the waveform digitizer to

record all radiation interactions within the detector. From this information, gamma-ray interactions can be extracted and digitally assigned to a pulse height spectrum. While the half analog/half digital system is a powerful tool for analyzing all pulse types from a BC-523a based detector, it does have some significant drawbacks. The greatest disadvantage for such a system is that it uses between 6 and 8 NIM's which increase cost, increase size, and decrease reliability. This analog circuitry can be completely eliminated if an all-digital system is used.

The Oregon State University BC-523a detection system uses an all-digital system as diagrammed in Fig. 4. The system is made up of only four pieces of physical equipment: the detector (and PMT), high voltage power supply, waveform digitizer, and a personal computer. The waveform digitizer will record the pulses while the PC will run the control algorithm (written in Matlab). This control program will perform the pulse shape analysis, qualify neutrons that deposit all of their energy inside the detector, apply the neutron reconstruction algorithm, and output neutron counts, neutron spectra, gamma counts, and gamma spectra.

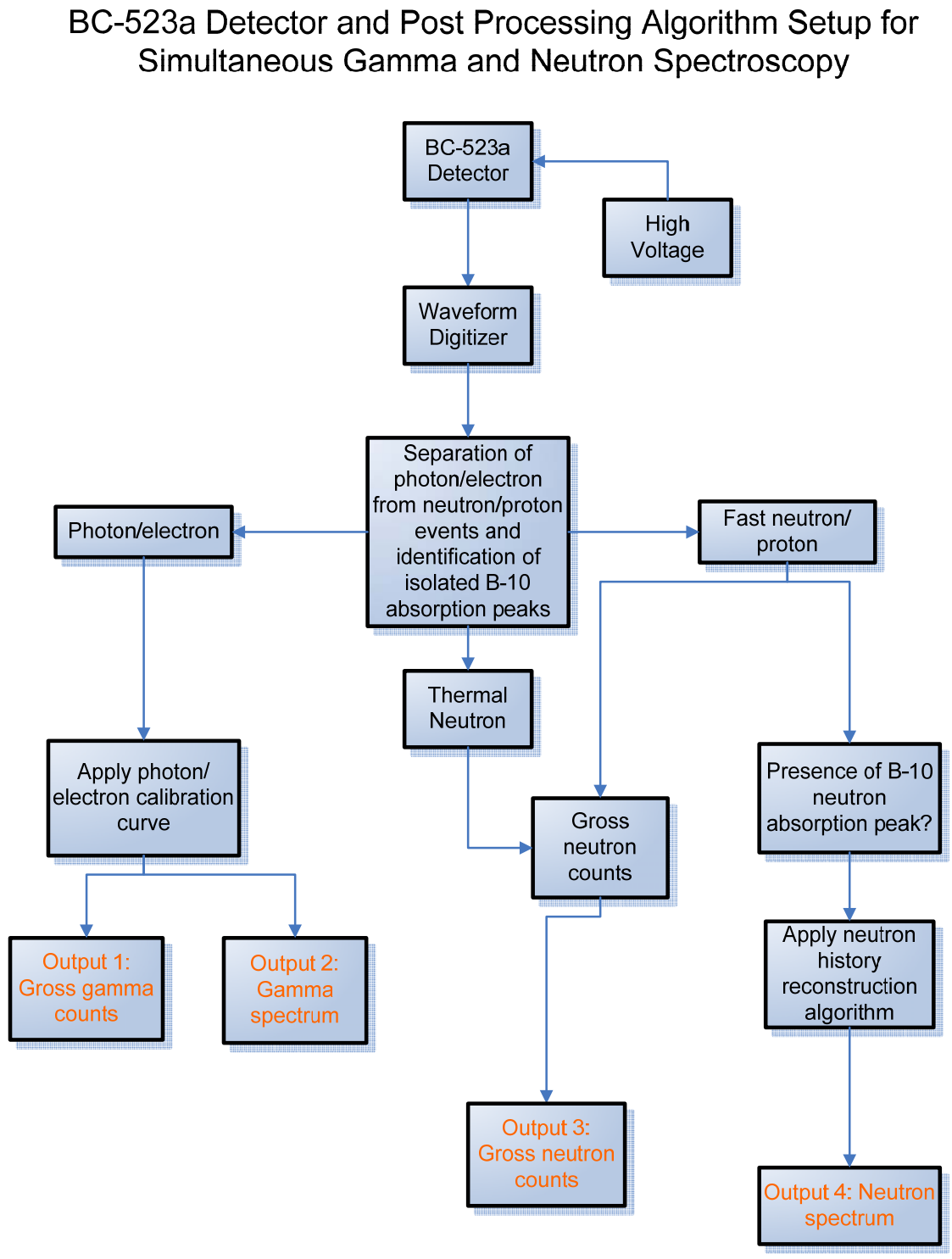

Fig. 4. Detector and algorithm set-up.

3.3.1 Digital Pulse Processor

A valid pulse is recognized, by the digitizer, once the output of the anode exceeds a specified voltage. When this condition is met, the signal begins to be recorded a short time before the pulse starts using a pretrigger. The signal leaves the detector anode, and then to a low-pass Nyquist filter (in order to satisfy the Nyquist-Shannon theorem) so that the detail of the signal is preserved. The analog signal is then digitized by a 12 bit/ 200 MHz analog-to-digital converter. Each signal is 1024 time steps long, with each time step equal to 5 nanoseconds, yielding a total pulse sampling duration of 5.12 microseconds. Once the pulse is digitized, it can be stored in an array in Matlab for off-line manipulation and it can be processed on-line to construct real time spectra.

3.3.2 Matlab Control Algorithm

The ultimate result of the Matlab pulse processing algorithm is to yield real-time low-resolution (but energetically accurate) neutron and gamma spectra. It is important to note that the gamma spectrum will contain no photopeaks given the extremely small photoelectric interaction probability for a low-Z detector material. The gamma spectrum will more likely be condensed into a gross gamma-ray count output. For this to be accomplished, the two pulse types must be identified consistently in any given pulse sample.

Gamma-ray and neutron signal pulses will be differentiated from each other based on the difference between their fall times. That is to say for pulses of the same amplitude, gamma-rays will consistently scintillate faster than neutrons. Each pulse

will have associated with it a prompt scintillation (fluorescence) and a delayed scintillation (delayed fluorescence). This difference in scintillation times (or pulse decay times) can be quantified by determining the ratio of the total charge generated from the prompt scintillation and the delayed scintillation (Moszynski 1991). This begs the question of how best to accomplish such a double charge integration pulse shape discrimination technique. The most significant problem associated with the charge comparison method will be the execution of baseline subtraction. The baseline will always be shifting and, if the baseline subtraction is not near perfect every time, the relatively small delayed scintillation component of the pulse will be skewed, if not altogether lost in the noise of an ever-shifting baseline. The solution is to use a series of filters to separate out the fast and slow scintillation components of every pulse by integrated different sections of the incoming pulses. (Farsoni 2006, Jordanov 1994 (2)).

The filter itself is essentially a symmetric bipolar step function that serves to integrate the pulse coming from the PMT anode. It is the convolution of this filter and the signal pulse that produce the characteristic trapezoidal shape where the maximum amplitude of the trapezoid is the total integrated charge. The advantage of this type of filter is that the baseline is removed, the height of the trapezoid is proportional to the integrated charge of the pulse, and any ballistic deficiting effects are removed (Jordanov 1994 (2)). The ability to filter out a prompt and delayed signal (fluorescence and delayed fluorescence signal) is facilitated by changing the characteristics of the filter itself. To extract a signal from a scintillation pulse containing multiple time components, a single filter of length L will be implemented.

The value of L will be approximately 2-4 times the decay time of the scintillation component of interest.

In order to quantify the prompt and delayed components of any given scintillation pulse, two filters whose lengths correspond to 2-4 times the prompt and delayed scintillation decay time will be used. One additional filter must be used to detect the boron capture peak. The length of this filter, which is close to the length of the prompt scintillation filter, will be on the order of the time profile for the boron capture pulse. The boron capture pulse is also made up of a prompt and decay component. However, the boron capture filter is not intended to identify the boron capture pulse by measuring the ratio of prompt and delay scintillation. Although this method is theoretically possible, the boron pulse amplitude is so small that statistical noise will likely make this method impractical. As a result, the boron capture filter is designed to measure the amplitude of a "potential" boron capture event over a time where a boron capture is likely.

Due to the fact, that the vast majority of boron capture pulses are nearly identical in height (about 60 keVee), a simple pulse height window can be established to identify boron capture events (Aoyama 1993), minimizing the risk of falsely identifying a recoil neutron or gamma-ray as a boron capture event. If this boron capture peak is identified, a pre-trigger method will be used to examine the waveform occurring, in a given time window, prior to the boron capture peak. This pre-trigger window is intended to find prompt scintillation peaks. The duration of this window is based on the average time it takes for a neutron to be absorbed in the detector. If a boron capture peak is identified and there is no preceding prompt scintillation pulse in

the given time window, it is reasonable to say the pulse was simply a thermal neutron absorption. Hence the neutron was at thermal equilibrium when it entered the detector and the pulse should be tallied as a neutron count. However, if the boron capture peak is identified and it has a prompt scintillation pulse preceding it, one can say that particular neutron deposited all of its kinetic energy within the detector and was then absorbed. Once it has been determined that a neutron count indeed contains energy deposition information, the neutron history reconstruction algorithm can be implemented. Once the corrected energy is known, the neutron spectrum can be updated.

The pulses that are identified as gamma-rays will undergo a simple one-step process where a calibration curve, that relates pulse height (voltage) to gamma ray energy, will be applied. A gross count rate of gamma-ray interaction will also be tallied by the algorithm.

3.4 The PuBe Source

3.4.1 The PuBe Neutron Energy Spectrum

In order to evaluate the success of the neutron history reconstruction algorithm, a known neutron source must be used. Once a sufficiently large number of pulses are recorded, the algorithm must assign new neutron energies to each neutron so that the overall energy spectrum is reproduced. For this purpose a 3 Ci PuBe source will be used. This source was constructed using 48 grams of plutonium and 24 grams of beryllium powder. This powder was scintered between a center tantalum cylinder and an outer stainless steel cylinder. The source generates neutrons via an alpha-neutron

reaction; the alpha particles originate from the plutonium. This is, essentially, a monoenergetic source, however as the alpha particles move through the surrounding material they lose kinetic energy. The result is alpha particles incident on the target beryllium atoms that range from zero kinetic energy to the original monoenergetic alpha particle emission energy. Once an alpha particle interacts with a beryllium atom, the alpha particle may be absorbed if its kinetic energy matches the energy needed to excite the resulting ^{13}C atom to one of its resonance levels. The excited ^{13}C atom (typically) decays to either the ground state or to a 4.43 MeV excited state, through the emission of a neutron. The energy of the resulting neutron is dependent on the excited state from which it came. However, this de-excitation does not produce monoenergetic neutrons; it produces a distribution of neutron energies with some peak energy. It is this combination of excited states and distribution of neutron energies that produces a complicated neutron emission energy spectrum with reasonably well defined peaks (Lehman 1968).

Several studies were undertaken throughout the 1950's and 1960's to characterize this energy spectrum. One such study characterized an 80 gram PuBe source using a neutron sensitive film emulsion with a random-drift scanning technique (Lehman 1968). This study yielded a neutron energy spectrum as reproduced in Fig. 5.

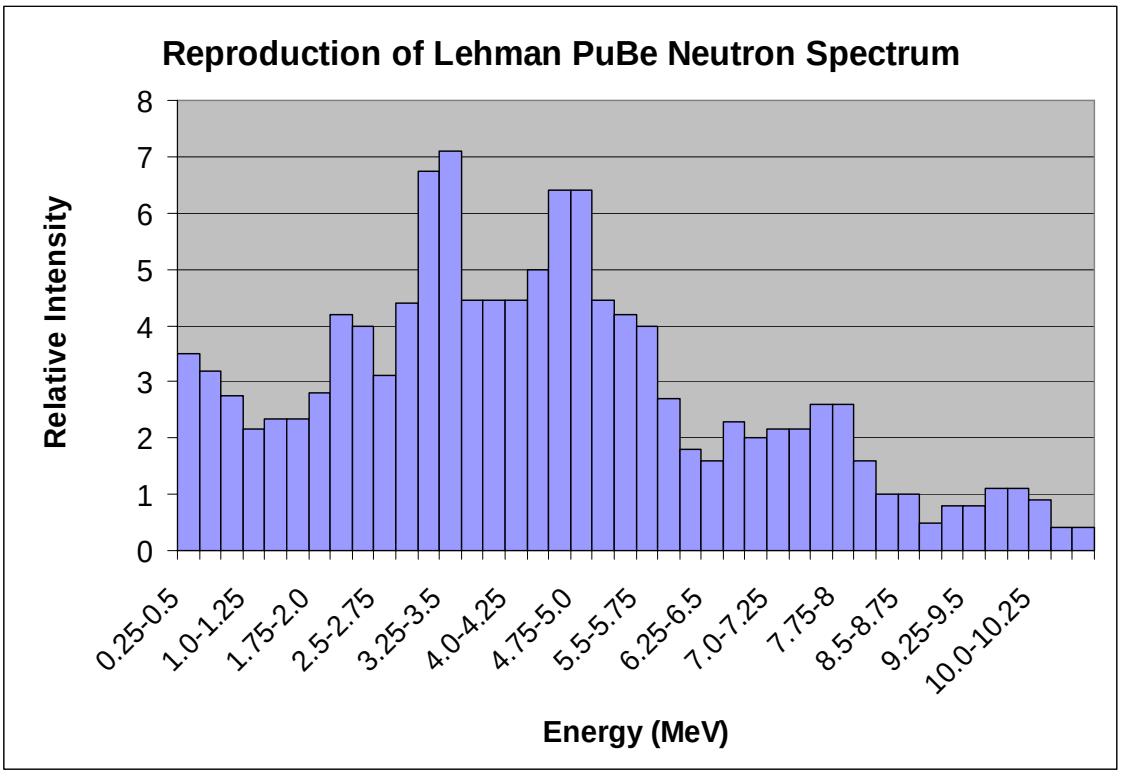

Fig. 5. Lehman PuBe neutron spectrum

The most important features of this spectrum are the peaks at 2.3, 3.2, 4.8, 6.6, 7.8, and 9.8 MeV. This spectrum is in close agreement with other similar studies (Anderson 1971).

The PuBe source was chosen, largely, due to the complexity of its neutron energy spectrum. It is felt that if a complex neutron energy spectrum can be reproduced, then the validity of the neutron history reconstruction algorithm will be confirmed.

3.4.2 Factors that Alter the PuBe Neutron Energy Spectrum

Unlike typical radiation sources (gamma-ray, beta, alpha, etc.) the PuBe neutron energy spectrum should not be thought of as constant in shape from source to

source. This stems from the fact that within the source itself there are a number of nuclear reactions that are dependent on an ever-changing atomic composition within the source. The intended outcome is the (α,n) reaction, however elastic scattering of neutrons by beryllium, (n,2n), and neutron induced fission of plutonium, can also take place, both of which will alter the shape of the neutron energy emission spectrum. As the source gets older, the small amount of ^{241}Pu will grow into ^{241}Am, and as a result there will be an increase in the neutron emission rate from ^{241}Am, due to its relatively large fast fission cross section. Therefore, the increase in neutron yield in any PuBe source will be from the (n,2n) reaction and the fast and thermal neutron induced fission of plutonium or americium. Fortunately, all of these other reactions will produce neutrons of relatively low energy (approximately 1-2 MeV), and will only increase the total neutron yield of the source by 6-30%, depending on the size and age of the source. The end result is that all PuBe sources will have an elevated output below 2 MeV, leaving the rest of the neutron energy spectrum relatively independent of the factors discussed above (Anderson 1972).

3.4.3 Neutron Transport within the Laboratory

It is important to consider that the Lehman (1968) neutron emission spectrum is a source term and is not the same as the expected detector response. In order to move from a source term to detector response, the neutrons must be transported numerically in their environment. Furthermore, the intrinsic efficiency of the detector and the statistical variation associated with the system must be taken into account when modeling detector response. Simulations will be carried out using MCNP5, the

Lehman spectrum, and the 12.7 cm diameter 7.62 cm deep BC-523a detector. The neutron spectrum will be estimated using a flux tally along with a boron absorption tally modification. Although this tally records the flux as a function of energy, when coupled with the boron capture modification it records the neutron absorption in boron and the energy at which that neutron entered the detector. This, essentially, tells us the probability of the neutron depositing all of its kinetic energy inside the detector, and of being absorbed by ^{10}B as a function of incident neutron energy.

The surroundings of the detector will not change the intrinsic efficiency of the detector; however the surroundings will alter the energy spectrum incident on the detector, which will contribute to the difference between the emission spectrum and detector response. The benchmark that will be used to validate experimental results will be Lehman's spectrum, after it has been "transported" by Monte Carlo simulation of the room in which the experiment is carried out. For the MCNP benchmark the detector will be placed in the center (50 cm away from the source and 10 cm off the ground) of a 2.1 m wide by 3.6 m deep by 3.6 m tall room surround by 30 cm of concrete. This room (a decommissioned X-ray room in the OSU Radiation Center) is a room where neutrons will be heavily back scattered into the detector, resulting in an energy spectrum shift to lower energies.

3.5 Additional MCNP Simulations

3.5.1 Non-Hydrogen Collisions

The atomic composition of the BC-523a will be used as input for MCNP. Then, a specialized tally will be used to calculate the number of collisions per atom

type (hydrogen, oxygen, carbon, and boron) as a function of neutron energy. The detector will be simulated such that it is infinitely large. This ensures all neutrons are absorbed (primarily by boron) instead of having some neutrons leave the detector. This in turn, results in the non-hydrogen correction being performed for neutrons that lose all of their energy within the detector's active volume; in other words, the correction will only be performed on neutrons that carry an incident kinetic energy. Once the average number of collisions per atom type is know, the average fractional loss per atom type can be calculated and then the total neutron fractional energy loss can be assessed.

3.5.2 Inelastic Scatter Photons

A two step process is used to correct for the potential signal loss that will result from photons, created by inelastic neutron scattering, that leave the detector. The first step is to create an infinitely large detector in MCNP and tally the number and energy of inelastic scattered photons generated as a function of incident neutron energy. Once again, an infinitely large detector is used because our interest is correcting the energy of fast neutrons that are thermalized and absorbed within the detector. The second part of the correction is to model a BC-523a detector of actual size (12.7 cm diameter by 7.62 cm deep) with a uniform gamma source of an intensity and energy as determined in the first step. From this, the fraction of energy that leaves the system from inelastic-scatter photons can be mapped out as a function of incident neutron energy.

3.5.3 Intrinsic Neutron Absorption Efficiency

In order to transition from ideal detector response to neutron emission spectral flux, the intrinsic neutron absorption efficiency must be calculated. This efficiency is a function of detector composition and geometry. To a lesser extent the geometry of the source will affect the intrinsic efficiency. To determine inelastic neutron absorption efficiency, a neutron source was simulated as a point source one meter away from the center of the face of the detector. A special tally was used to tabulate the probability that a neutron will be absorbed in ^{10}B as a function of neutron energy.

3.5.4 482 keV Capture Photon Effect

Upon absorption of a neutron the, ^{10}B nucleus becomes a compound ^{11}B nucleus. Only six percent of the time does this compound nucleus decay to a ground state ^{7}Li nucleus and an alpha particle. The remaining 94 % of the time the compound ^{11}B nucleus decays to an excited ^{7}Li nucleus and an alpha particle. This excited ^{7}Li nucleus rapidly decays by the emission of a 482 keV photon. It is possible that this photon will be deposit energy within the detector. The extent of this effect needs to understood.

This MCNP experiment is similar to the inelastic scattered photon experiment in that actual detector geometry is used with a uniform gamma-ray source distributed throughout the detector's active volume. The gamma-ray energy is mono-energetic at 482 keV. The energy deposited by these 482 keV photons is then tabulated.

3.6 Calibrations

3.6.1 Characterization of Gamma and Neutron Pulses

In order for any pulse-shape discrimination method to succeed, one must be able to characterize the shape of the pulses that are likely to be encountered during typical operation (gamma rays, neutrons, and boron capture pulses). Gamma-rays and neutrons will be characterized in terms of prompt and delayed scintillation via the use of fast and slow trapezoidal filters. These characterizations will be recorded as a function of pulse amplitude, which then can be related back to pulse energy.

Gamma-ray pulses can be detected, digitized, and stored electronically by using a standard 1 micro Curie check source of ^{60}Co for a sufficiently large number of counts. It is unlikely that the detector will require shielding from background neutrons, given their extremely low flux.

Characterization of neutron pulses is more complicated because it is difficult to achieve a very low background gamma-ray component. In order to best compensate for the non-trivial gamma-ray background, the PuBe sources will be heavily shielded and all other sources will be removed from the laboratory. Neutrons will be identified not by their pulse shape (due to the fact that this is what is being measure), but they will be identified by the presence of a delayed boron capture peak.

The final characterization will be of the thermal capture of a neutron in ^{10}B. This characterization is important in the correct identification of the delayed scintillation pulse. The identification will be accomplished using the same experimental set-up as the fast neutron pulse characterization, except that the PuBe source will be placed next to a large polyethylene volume so that a large fraction of

the fast neutrons become thermalized, resulting in abundant ^{10}B thermal capture pulses.

3.6.2 Gamma-Ray Calibration

Gamma-ray calibration will be carried out similar to a standard gamma-ray calibration, with one major exception. The calibration will use standard gamma-ray check sources with distinct mono-energetic photons (^{60}Co, ^{137}Cs, ^{54}Mn, and ^{22}Na). These sources will be placed, individually, dead center at the face of the detector and the resulting spectra will be recorded. Due to the near zero photo peak cross section for such a low Z detector, it is not possible to calibrate detector output voltage to photo peak channel number (or photo peak energy). Instead, the calibration must be made using the next most distinctive feature of the spectra, the Compton edge.

3.6.3 Neutron/Fast Proton Calibration

The scintillation response function of protons in BC-523a is of paramount importance when conducting the neutron history reconstruction algorithm. This response function is dependent only on the scintillation material type and not on the detector geometry. Previous research (Aoyama 1993) has already determined this response function. This response was found to be:

$$L_p=0.328E_p^{1.5} \quad (17),$$

where L_p is the light output of a proton and E_p is the energy of the proton. Light output, L_p is expressed in terms of light units defined by Aoyama; our interest, however, is in the output voltage produced by proton energy deposition as a function

of energy. Fortunately, Aoyama's research also reports the electron response function in terms of the same light units. If the magnitude of pulses generated by fast electrons in both systems is known, they can be related to each other. It is in this way that the light output units (in Aoyama's system) will be replaced by an output voltage (in this system). This will yield the voltage output as a function of recoil proton energy needed for the neutron history reconstruction algorithm.

4. Results

4.1 Framework for the Implementation of the Neutron History Reconstruction Algorithm

When the simulations outlined in section 3.2 are carried out, the characteristic response function for 1 MeV incident neutrons in a purely hydrogenous organic scintillating material with an $E^{3/2}$ proton response function, predicts a median "recorded" energy of ~1.5 MeV and a maximum recorded energy that is nearly twice the actual incident energy (Fig. 6), if the neutron history reconstruction algorithm is not used. Needless to say, the overestimation of neutron energy is significant, making the use of uncorrected data in BGN spectroscopy highly questionable. An additional problem is the poor resolution (~20%) in the data due to the small number of charge carriers produced by neutron collisions and the non-linear response of the resulting recoil protons.

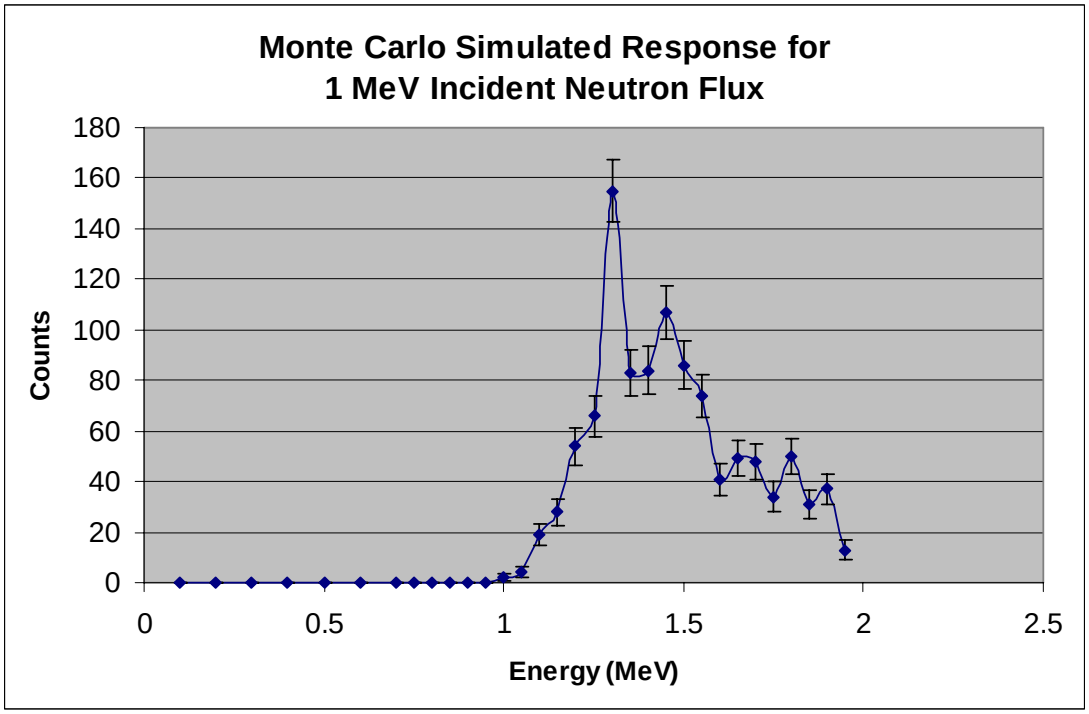

Fig. 6. Monte Carlo simulated response for 1 MeV incident neutrons.

Once the multi-collision and within-collision corrections (see Sections 3.1) are made, the characteristic incident neutron overestimation is reduced almost completely (Figs. 7 and 8).

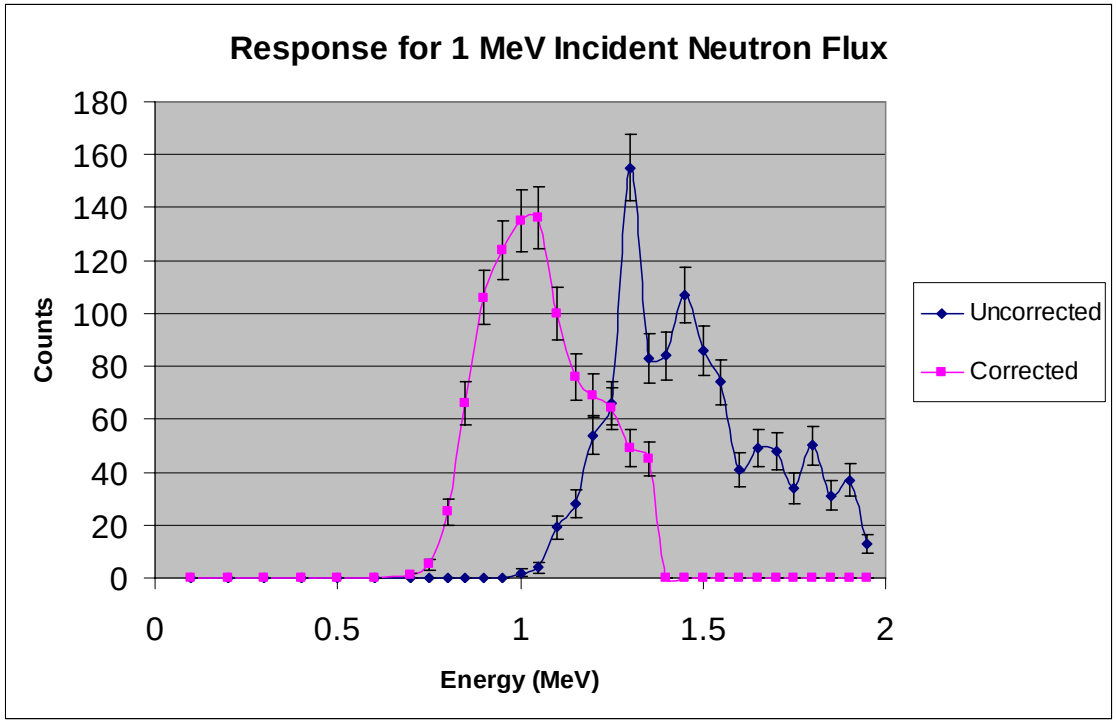

Fig. 7. Monte Carlo simulated response (corrected and uncorrected) for 1 MeV incident neutrons.

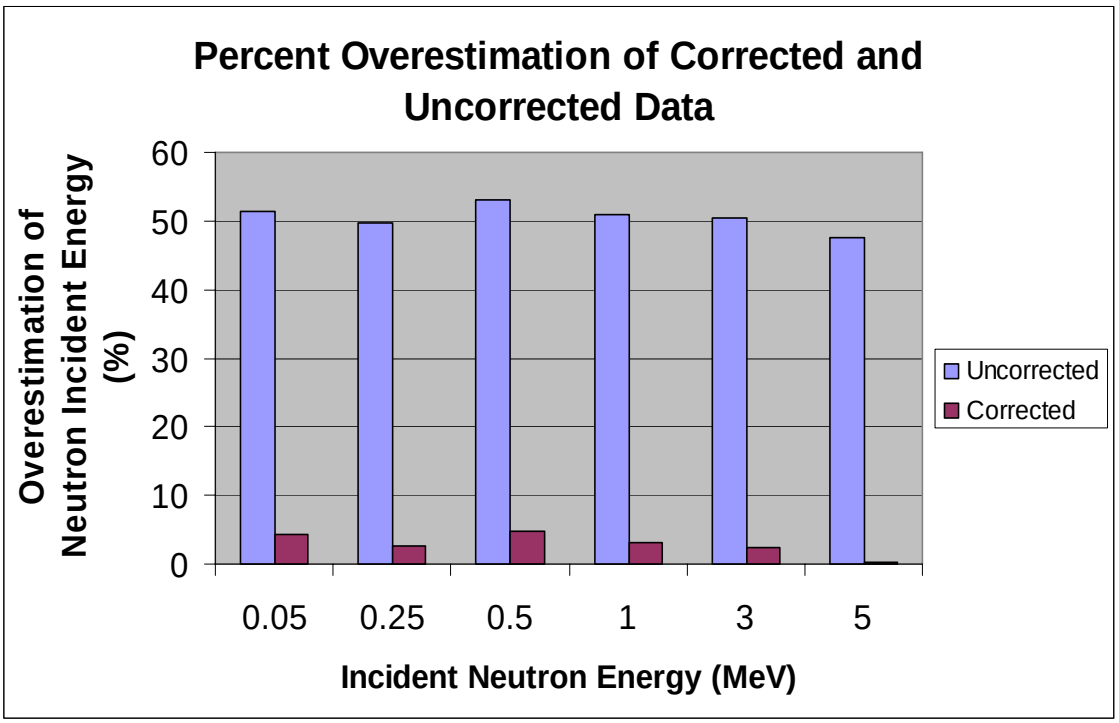

Fig. 8. Percent overestimation of corrected and uncorrected data.

While these results are encouraging, the effect that the reconstruction algorithm has on resolution is also significant as an average improvement of 33% was observed in the simulations (Fig. 9) between the corrected and uncorrected data.

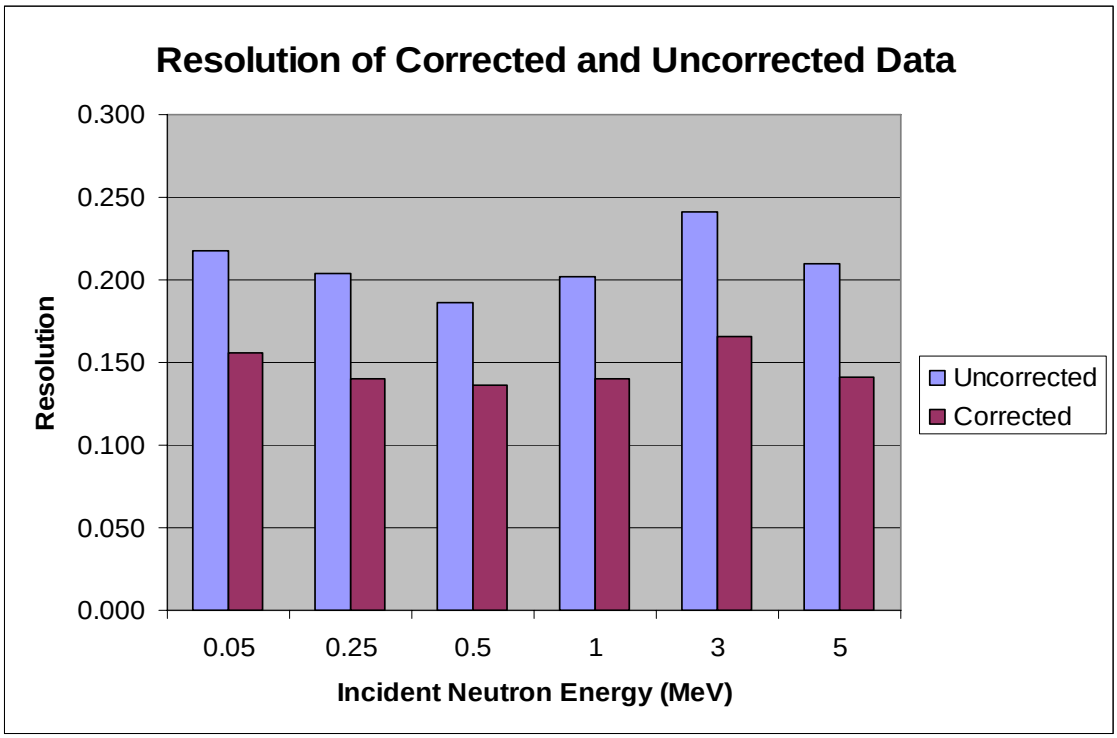

Fig. 9. Resolution of corrected and uncorrected data.

4.2 Sample Pulses

Below are a sample gamma-ray pulse (Fig. 10) and a sample neutron pulse (Fig. 11) recorded by the detection system. Both pulses show the general expected shapes in terms of fluorescence and delayed-fluorescence decay times, where the neutrons are characterized by a greater fraction of their total scintillation light output in the form of delayed-fluorescence.

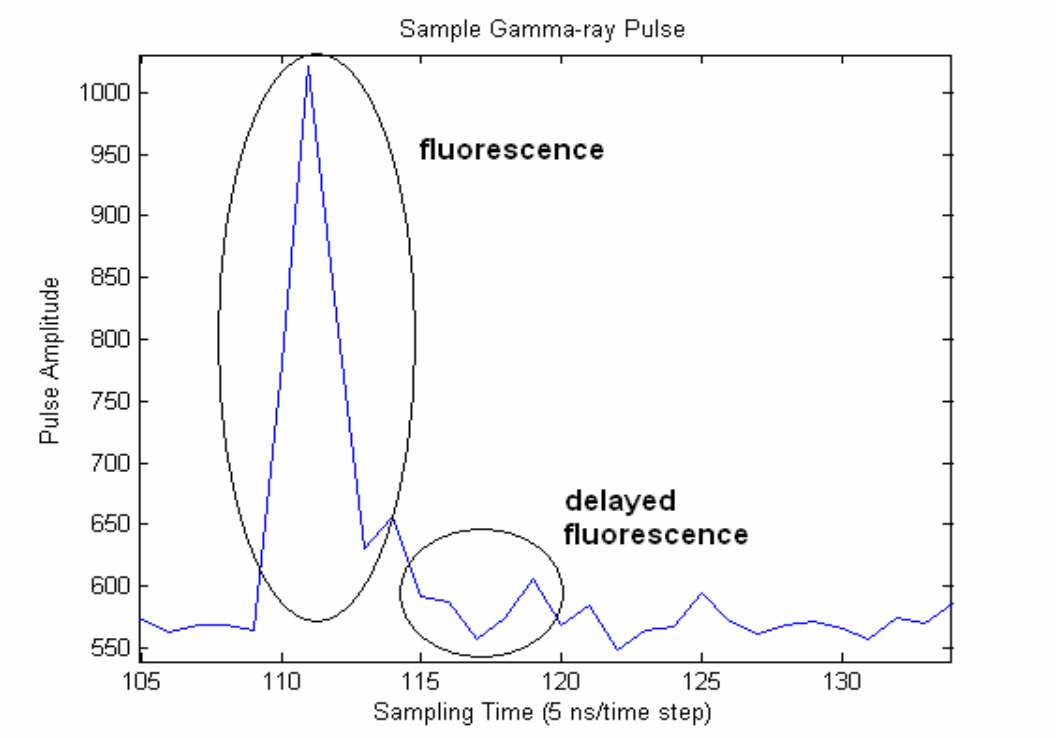

Fig. 10. Sample gamma-ray pulse.

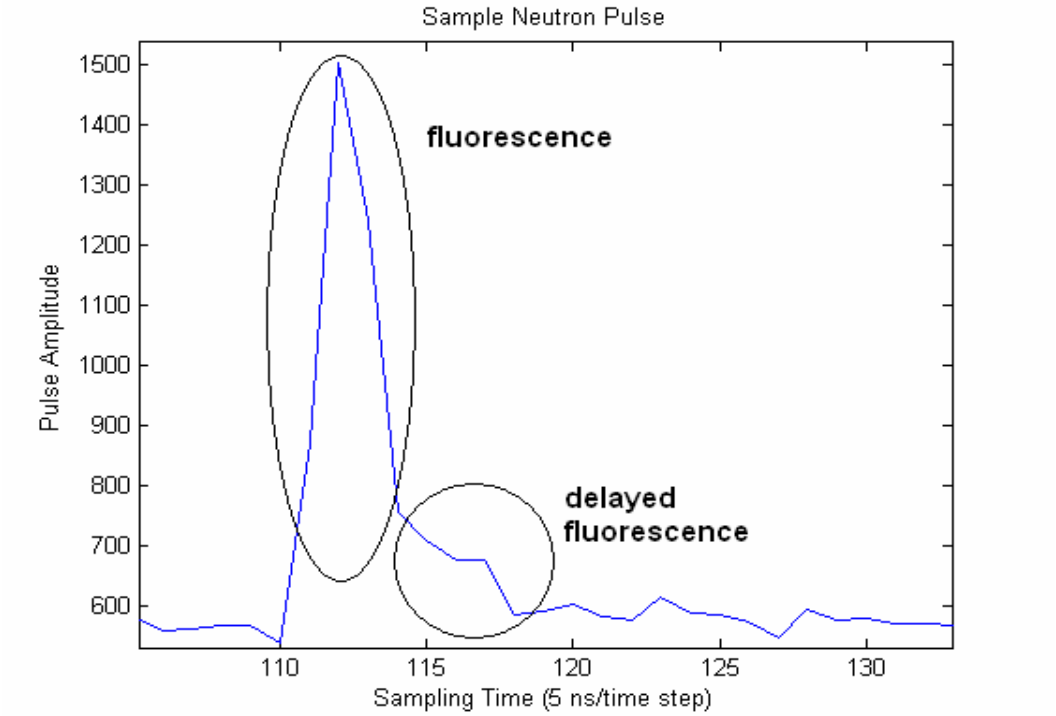

Fig. 11. Sample Neutron Pulse.

An example of the convolution of the integrating filter and a single pulse from the anode of the detector is provided in Fig. 12. The areas of the convolution resulting from the integration of the fluorescence and delayed fluorescence are outlined. The total integrated magnitude of the initial pulse is equal to the maximum of this convolution, occurring at approximately time step 135.

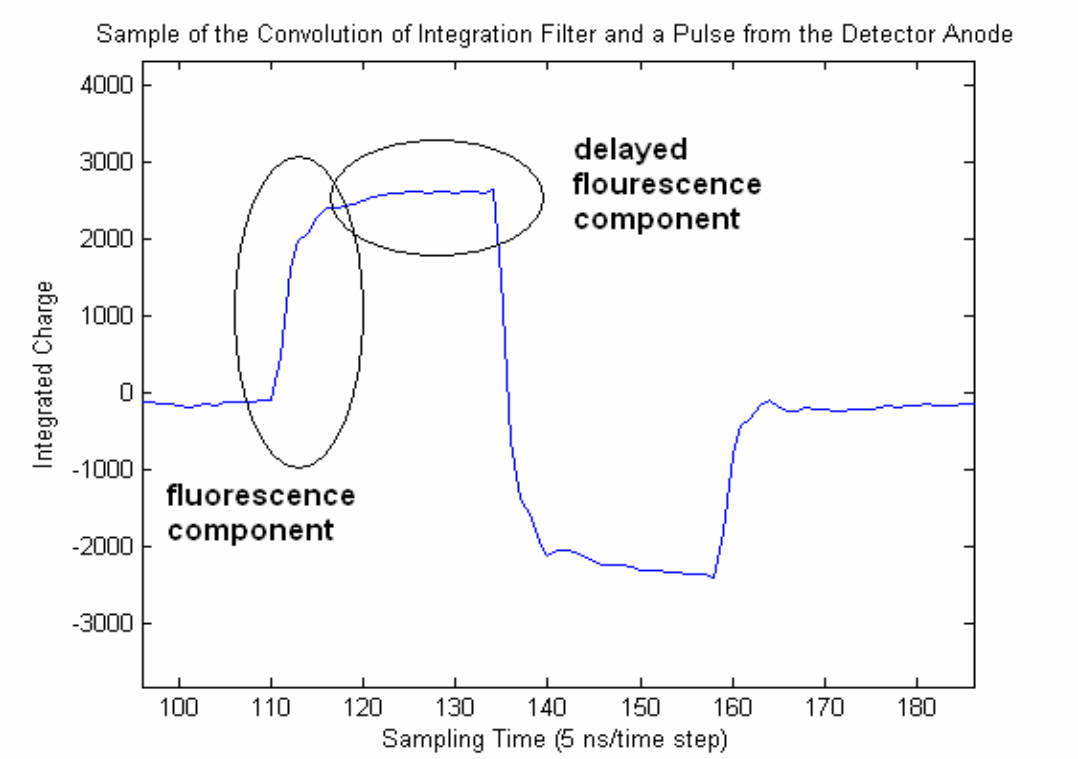

Fig. 12. Sample of the convolution of integrating filter and a pulse from the detector anode.

4.3 Gamma-Ray Energy Calibration

The gamma-ray energy calibration shows a strong linear relationship between the energy deposited by a gamma-ray inside the detector and the resulting light output (measured as an electrical signal at the anode), which is expected (Aoyama 1993). The light intensity is defined and recorded as the number of voltage steps exceeding

the baseline after the trapezoidal filter has been applied. One light unit was found to correspond to 0.000291 MeV, with an R^2 value of 0.9928. A sample recorded gamma-ray pulse height spectrum is provided in Fig. 13. It is important to note the predominant Compton edge, the absence of a photopeak, and the lack of pulse below the detection threshold of approximately 100 keV.

Table 1.1 Gamma-Ray energy calibration results

Isotope	Known Peak Energy (keV)	Measured Compton Edge Energy (keV)	Light Output (LU)
^{22}Na	511*	341	1300
^{137}Cs	662	478	1550
^{54}Mn	834.8	639	2300
^{60}Co	1250**	1038	3600

*energy of annihilation gamma-ray

**average gamma-ray energy

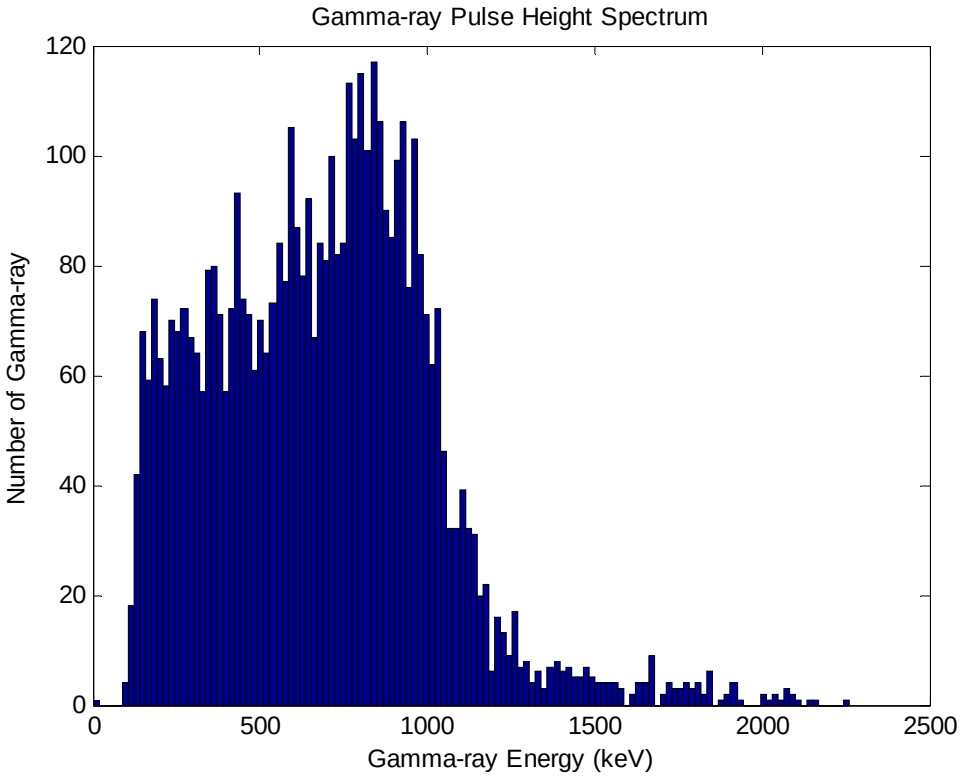

Fig. 13. Gamma-ray pulse height spectrum.

4.4 Neutron/Fast Proton Calibration

In order to carry out the neutron history reconstruction algorithm, the relationship between pulse amplitude (in laboratory light units) and the energy of a recoil proton must be known. This relationship, for BC-523a, is given to us by Ayoama (1993) in the following equation:

$$\text{Light Output}_{\text{Aoyama}}=0.328(E_{\text{proton}})^{1.5} \quad (18).$$

In scintillation experiments, the magnitude of the light unit will vary because it is defined differently by each researcher, usually in terms of some signal pulse amplitude. Aoyama defined his light units as:

$$1\ \text{Light Unit}_{\text{Aoyama}}=0.5\ \text{MeVee} \quad (19).$$

In order for Eqn. 18 to hold true for this research, the difference in the magnitudes of the two light unit values must be accounted for and the coefficient of proton energy (0.328) must be modified. This is accomplished by equating the light generated by fast electrons in Aoyama's experiment and in this research. If we equate Aoyama's light units to the light units in our detection system (using the gamma-ray calibration for this system of 1 light unit as being equivalent to 0.00159 MeVee, from Section 4.1) the following relationship emerges,

$$\frac{0.5 MeVee / LightUnit_{Aoyama}}{0.000291 MeVee / LightUnit_{OSU}} = 1724 \frac{LightUnit_{OSU}}{LightUnit_{Aoyama}}. \quad (20).$$

In other words, the light units for this experiment were 314 times smaller than in Aoyama's experiment. This relationship can be solved simultaneously with Eqn. (18) to relate OSU light units to recoil proton energy:

$$Lightoutput_{OSU} = 0.328 * 1724 \frac{LightUnits_{OSU}}{LightUnits_{Aoyama}} * (E_{proton})^{1.5}. \quad (21)$$

Finally, solving Eqn. (21) for the recoiled proton energy yields,

$$E_{proton}(MeV) = 0.00177(Lightoutput_{OSU})^{0.667} \quad . \qquad (22).$$

This calibration is system specific, i.e., the calibration is only valid for a single bias voltage applied to the PMT and for a single system gain as it is defined in the digital system configuration.

4.5 Average Neutron Response Function

Given below (Fig.14) are the data that describe the average neutron response for neutrons that deposit all of their kinetic energy inside the BC-523a scintillator. This response is constructed using the proton response function derived in Section 4.3 and the neutron history reconstruction algorithm method outlined in Section 3.1. This response function is reported in Fig. 14 without error, however it is important to note the reconstruction algorithm does have an associated uncertainty with it, as outlined in section 4.1. Furthermore this response is theoretical given that it is unlikely that any neutrons below 100 keV will produce any measurable scintillation pulse.

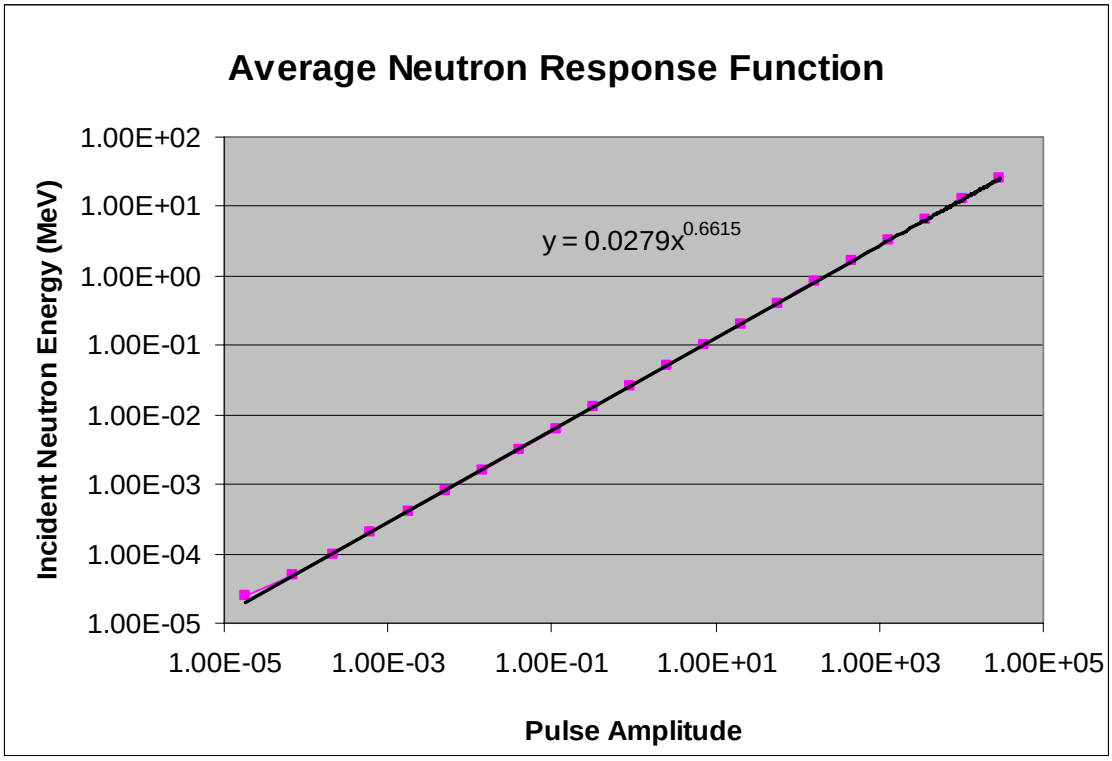

Fig. 14. Average neutron response function.

4.6 MCNP Simulations

4.6.1 Non-Hydrogen Collisions

The results from the MCNP simulations show a significant increase in the fraction of incident neutron energy that, on average, is imparted to non-hydrogen atoms as the neutron energy increases (Fig. 15). This increase is expected given that the scattering cross section for hydrogen falls off more rapidly with increasing neutron energy than the other elemental constituents of BC-523a.

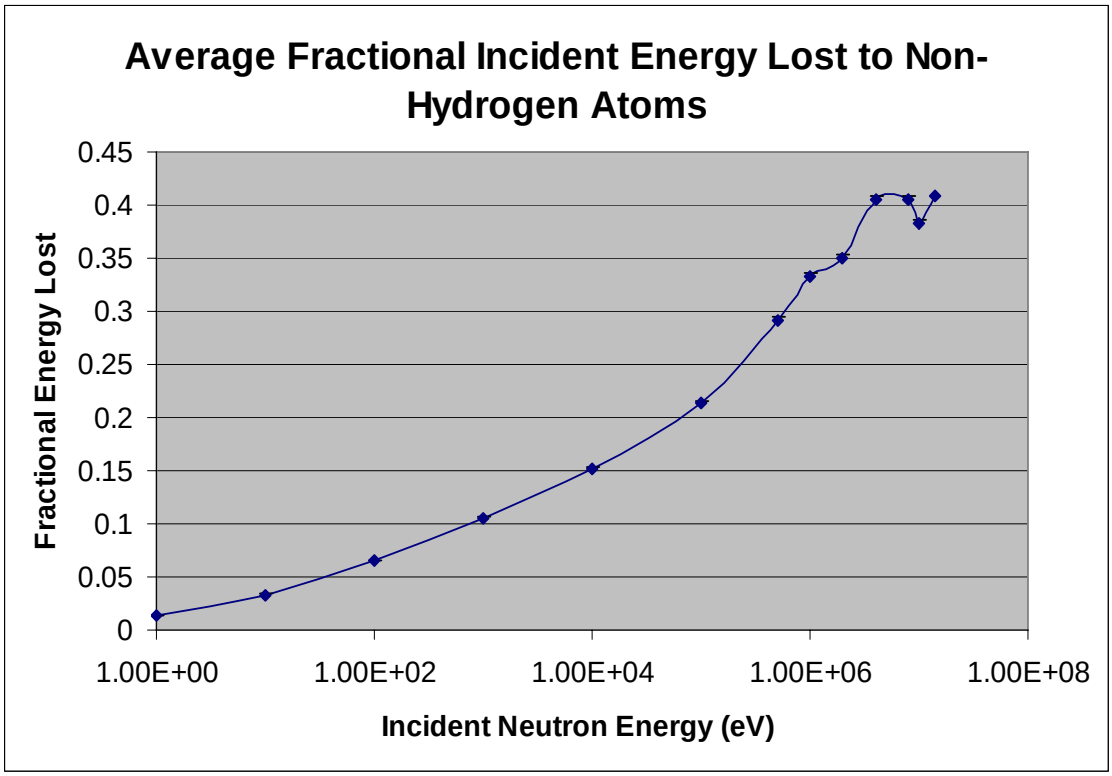

Fig. 15. Average fractional incident neutron energy lost to non-hydrogen atoms.

4.6.2 Inelastic Scatter Photons

Energy loss (as determined by MCNP) due to photons leaving the system from inelastic neutron scatter were found to be less significant (Fig.16) than the energy losses associated with the non-hydrogen collisions. This is also expected given that these are threshold reactions and that their cross sections are relatively small at any energy for low-Z materials.

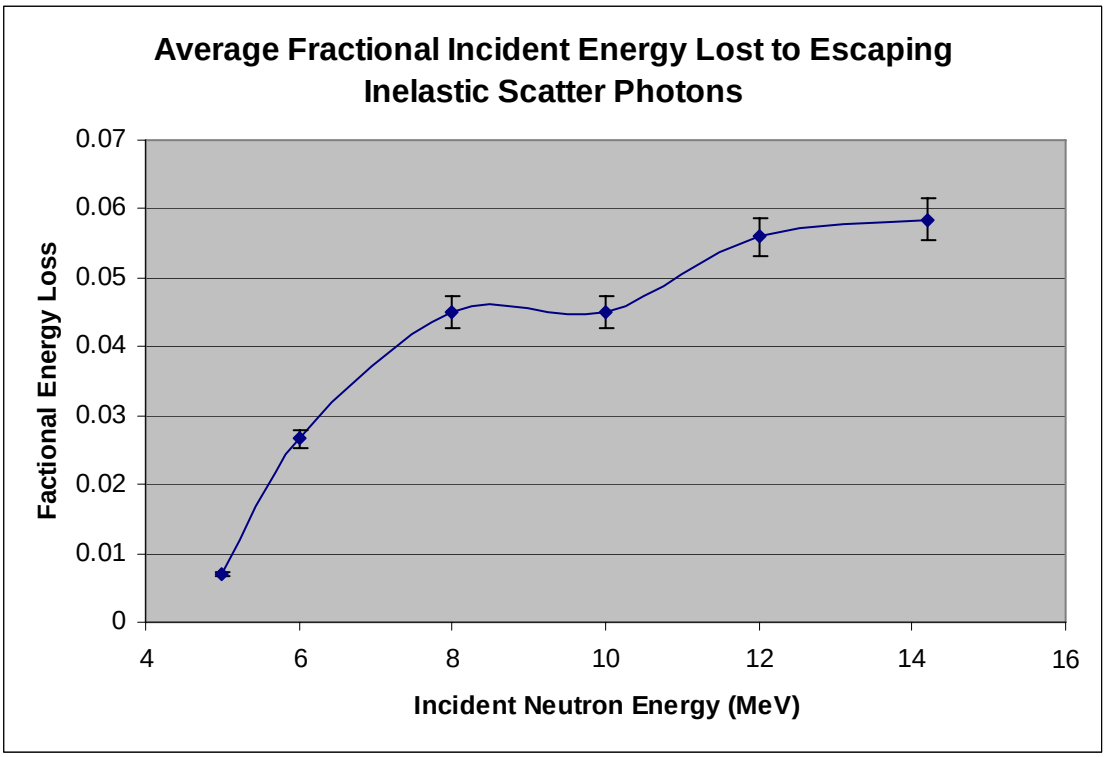

Fig. 16. Average fractional incident energy lost to escaping inelastic scatter photons.

4.6.3 Intrinsic Neutron Absorption Efficiency

The neutron efficiency (as determined by MCNP) for a point-source one meter away from the face of the detector was found to drop off rapidly with increasing neutron energy (Fig. 17). This is expected given that as neutron energy increases it becomes less likely that the neutron will thermalize and be absorbed by a ^{10}B atom within the detector volume. It is important to note that, the intrinsic efficiency was only calculated down to a neutron energy of 0.5 MeV; this is the approximate lower limit of detection for identifying fast neutrons. The intrinsic efficiency for thermal neutrons was found to be very close to unity.

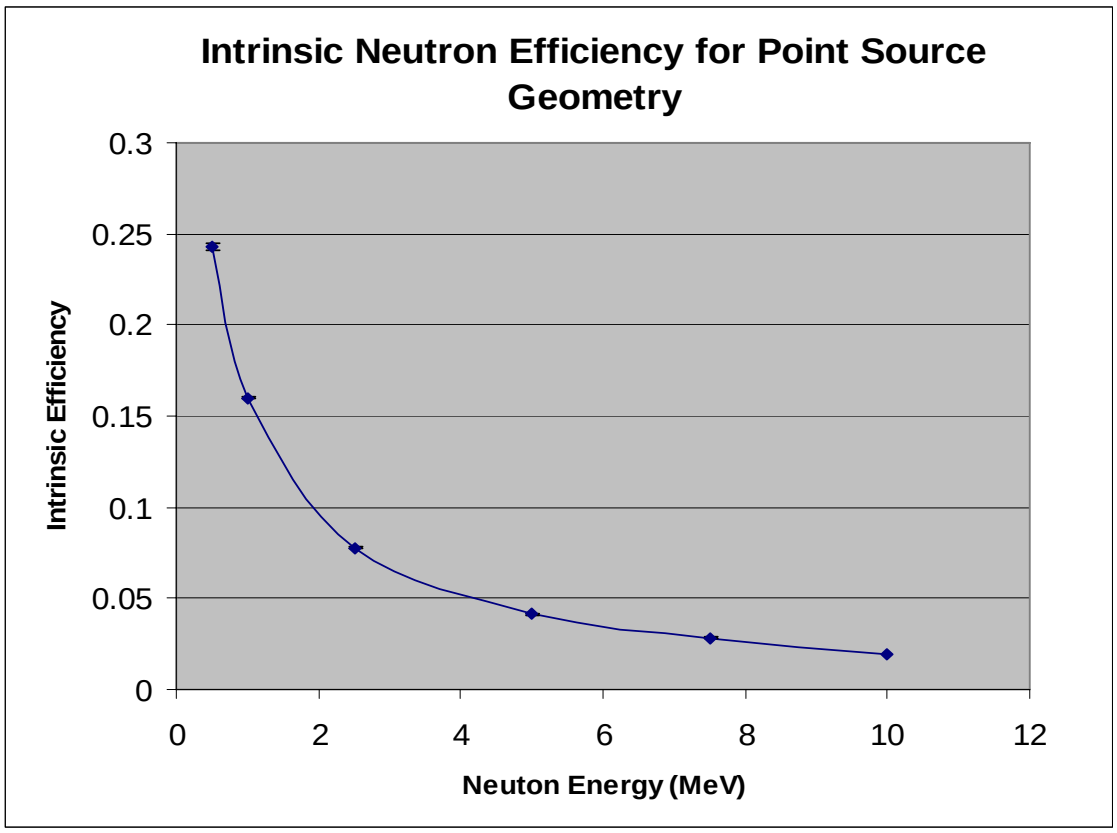

Fig. 17. Intrinsic neutron efficiency for point source geometry.

4.6.4 482 keV Capture Photon Effect

The MCNP simulation show that 72% of the time that there is a thermal neutron capture in the 12.7 cm by 7.62 cm detector; its pulse will be 60 keVee in magnitude. The remaining 28% of the time the resulting pulse magnitude is described by Fig. 18. The data show that if a 482 keV photon does interact within the detector volume, it will likely undergo a single Compton scattering event and result in a pulse between a magnitude of 320 keVee and 380 keVee.

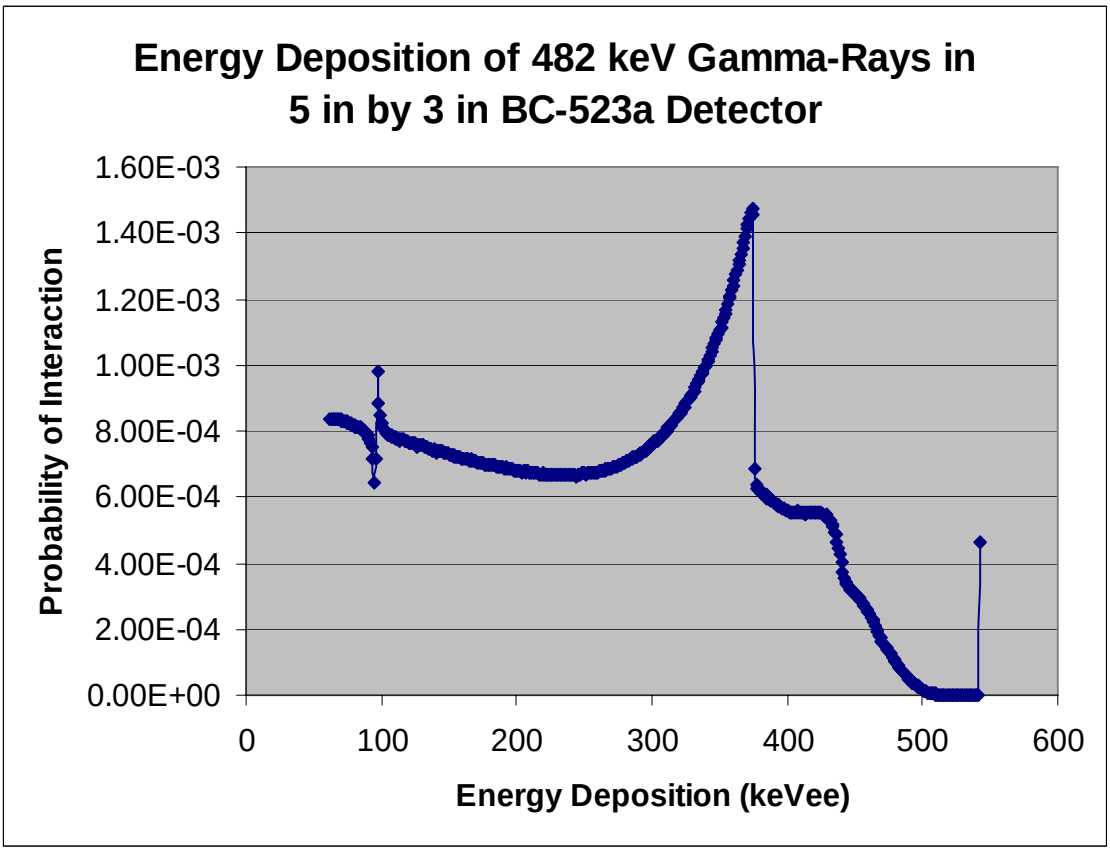

Fig. 18. Energy deposition of 482 keV gamma-rays and de-excitation of B-10 in a 12.7 cm by 7.62 cm BC-523a detector, when the 482 keV photon does not escape the detector.

4.7 Neutron Transport in the Laboratory

The results for the Lehman MCNP benchmark are given in Fig. 19. The results have been normalized so that the intensities are identical at a neutron energy of 2.0 MeV, to aid the visual comparison of the original and transported data. The results appear reasonable, as the expected response increases at very low energy (due to the thermalizing effects of the room) and the response decreases, with increasing neutron energy, due to the rapid decrease in intrinsic efficiency. The thermalizing effect of the room, coupled with the rapid decrease in efficiency, has the effect of removing all of the notable peaks in the neutron spectrum, except the peak near 2.0 MeV.

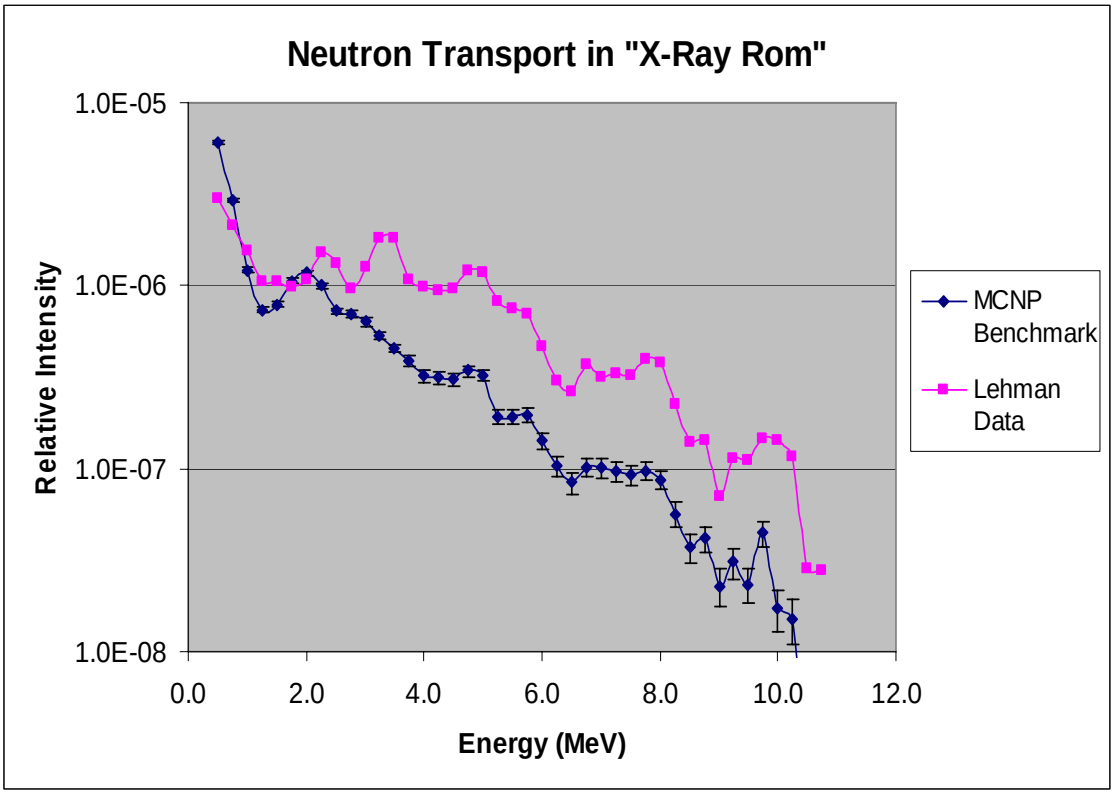

Fig. 19. Neutron transport in "X-ray room" as performed by MCNP.

4.8 Separation of Gamma-Rays and Neutrons

The double charge integration pulse separation technique (Section 2.4.2 and 3.2.2) shows the expected, general trends. The gamma-rays overwhelmingly have a fast-to-total charge ratio above 0.8 (Fig. 20). Due to the difficult task of creating a purely neutron radiation field, no similar results can be given for the fast-to-total charge ratio of only neutrons. However, the fast-to-total charge ratio of the PuBe source can be given (Fig 21). These results contain gamma-rays, fast neutrons scattering out of the detector, and neutrons depositing all of their kinetic energy within the detector. Because a large number of particles had a fast-to-total charge ratio less than 0.8, most of these are likely neutrons. This gives us some discrimination level between gamma-rays and neutrons. While these results are not as encouraging as

other charge separation experiments (D'Mellow 2007, Jastaniah 2003), the results are nonetheless reasonable given the relatively slow digitizer speed (200 MS/s). However, the double charge integration pulse separation technique should yield increasingly better results as digitizer speeds approach 1 GS/s.

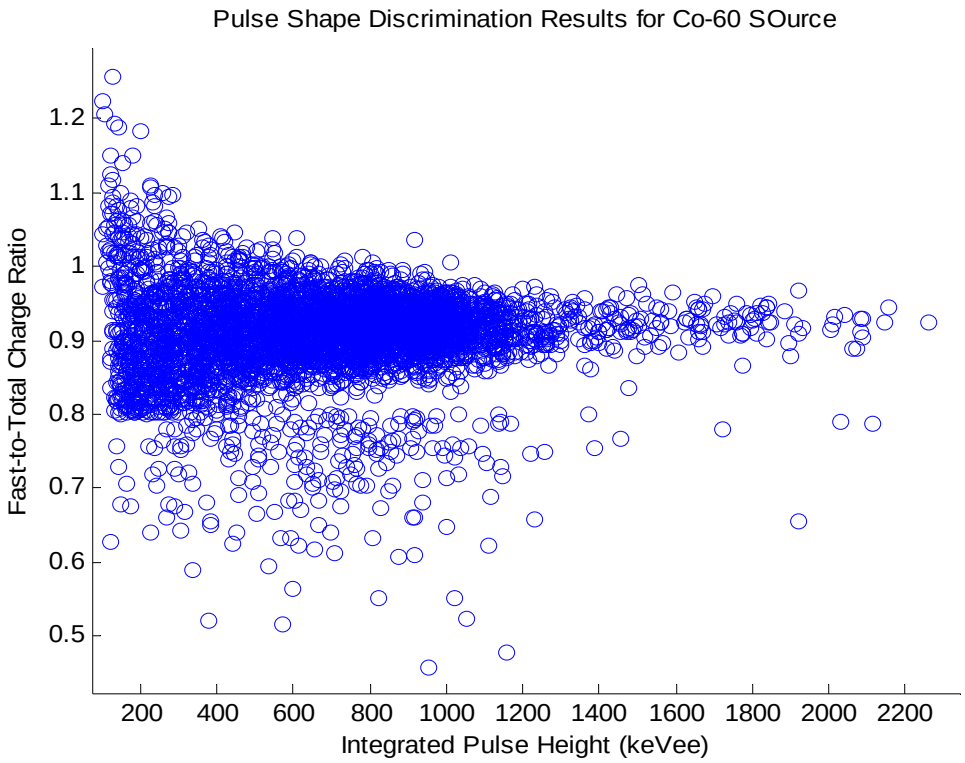

Fig. 20. Pulse shape discrimination results for Co-60 source.

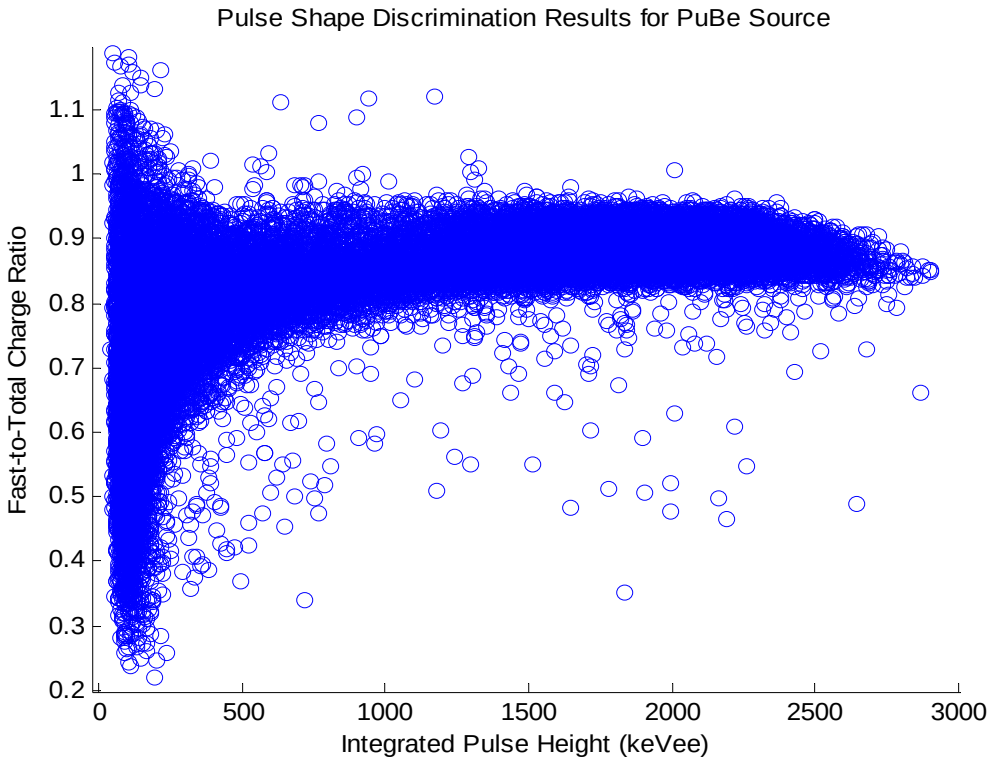

Fig. 21 Pulse shape discrimination results for PuBe source.

4.9 Background Neutron and Gamma-ray Spectra

Radiation background measurements (Fig. 22) were taken in the same laboratory as the primary neutron spectrum. The system was set so that a "neutron" was counted if the fast-to-total charge ratio was below 0.8 and if the delayed boron-capture peak was within 1.325 μsec of the prompt peak. The sample was 100,000 counts long, of which 39 were classified as neutrons. This low neutron count rate is expected given the presumably low level of background neutrons in the laboratory. Even if all neutron counts are false positives, they represent a rate of less than 1 in 2500 counts.

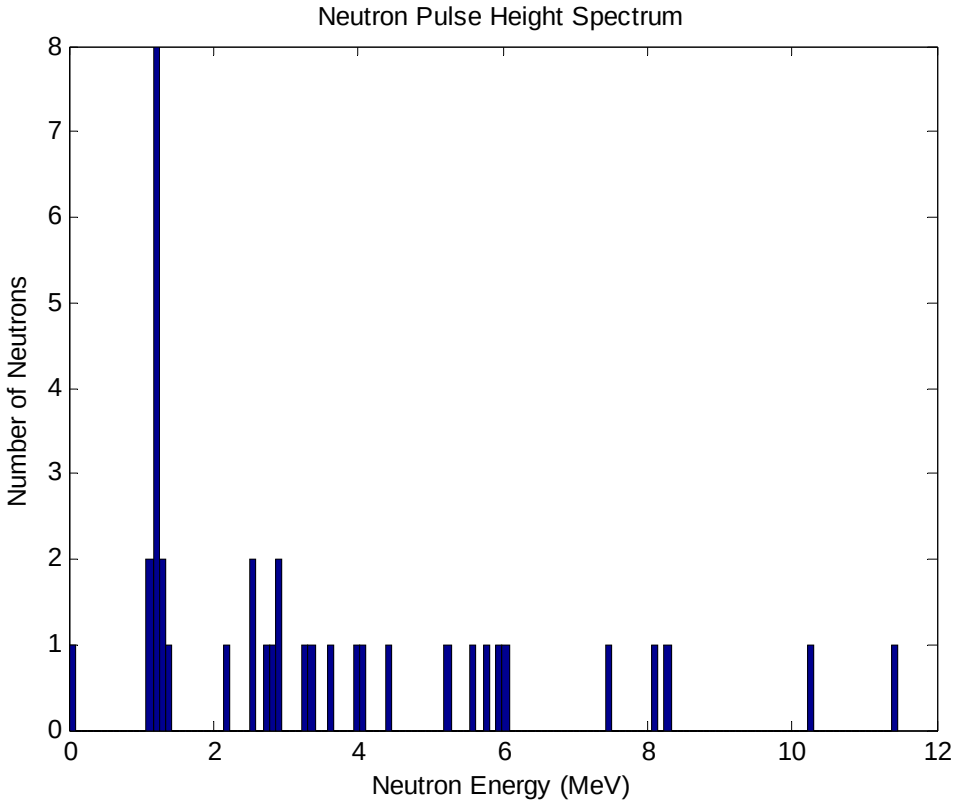

Fig. 22. Background neutron pulse height spectrum of the 523a detector.

The gamma-ray portion of the background, as seen in Figure 23, is made of three components. The first component is the check sources (^{137}Cs, ^{60}Co, ^{241}Am, etc.) inside the room. The second is from the decay chain of uranium that is naturally present in the concrete walls of the laboratory. The third component of this spectrum is the result of pulses caused by cosmic muons as they pass through the detector. It is important to note that true spectroscopy is not possible with this spectrum because of the low-Z detector material and that the vast majority of the gamma-rays undergo Compton scatter and do not deposit all of their energy within the active volume of the detector. The cosmic muons also do not deposit all of their kinetic inside the detector.

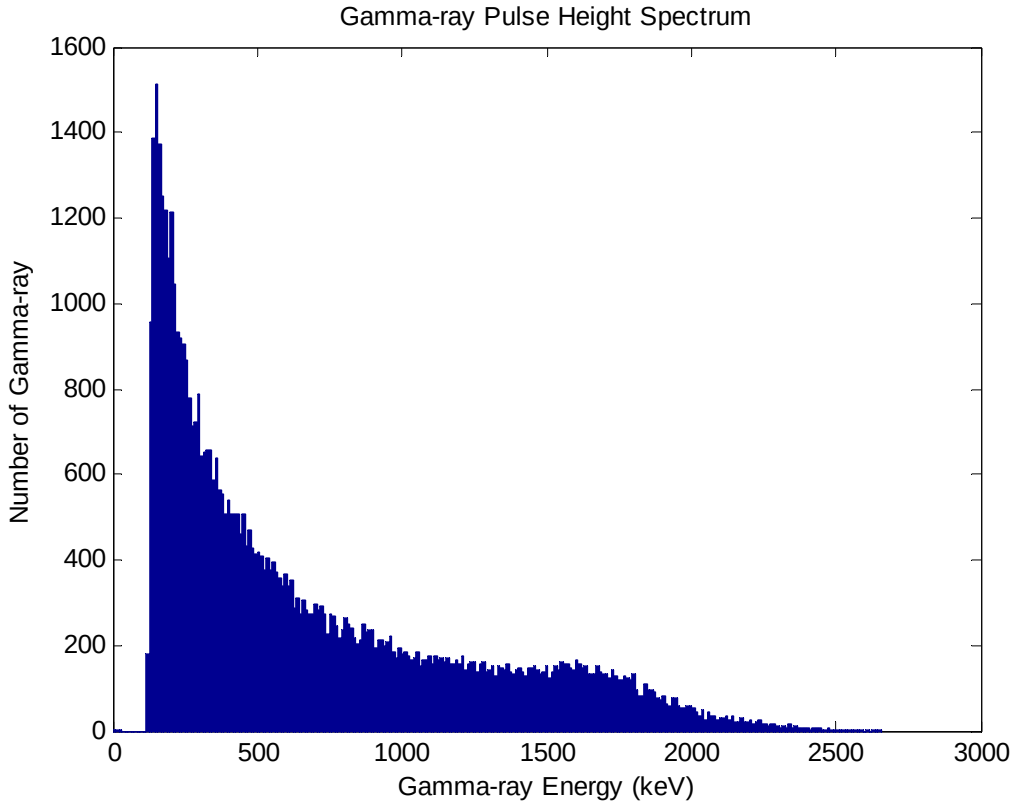

Fig. 23. Background gamma-ray pulse height spectrum of the BC-523a detector.

4.10 Measured PuBe Neutron Spectrum

The neutron reconstruction algorithm corrected spectrum below (Fig. 24) has a sample size of 10,000 neutrons. Each of these neutrons was qualified as a neutron with a fast-to-total charge ratio below 0.8 and its delayed boron capture peak within 1.325 μsec of the prompt peak. The energy resolution of this spectrum was set to match the Lehman neutron energy resolution.

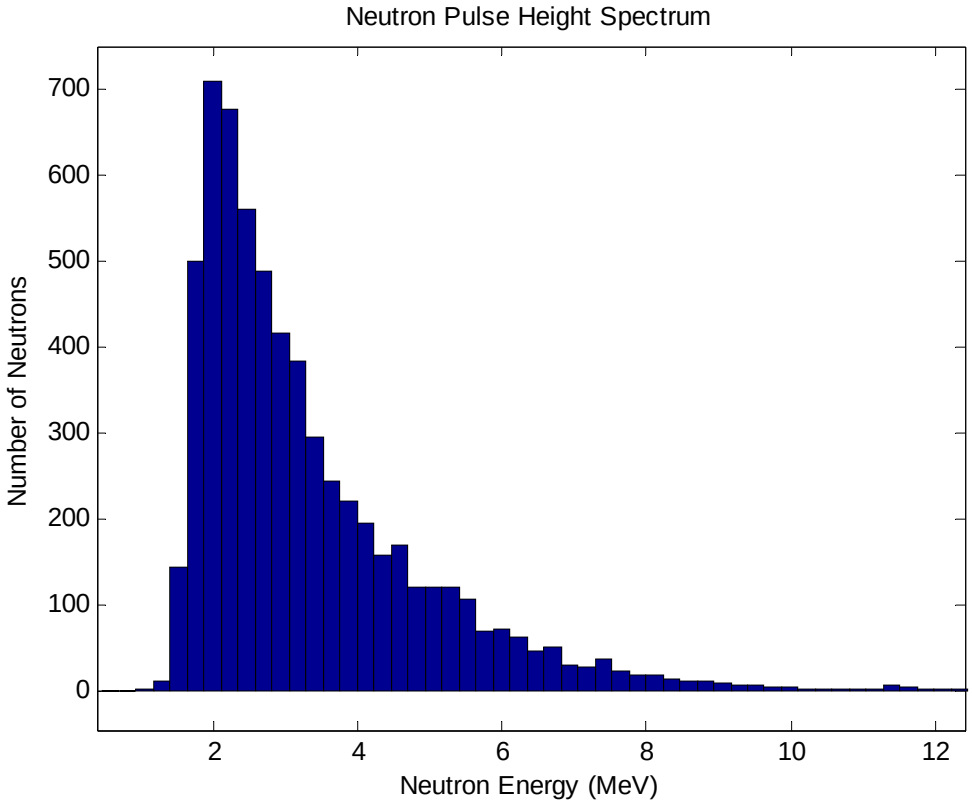

Fig. 24. PuBe neutron pulse height spectrum (48 channel) for the BC-523a detector.

The spectrum presented below (Fig. 25) is the same data as presented above (Fig. 24), except the energy resolution has been increased from 48 channels to 128 channels. The overall shapes of the spectra are the same, however a few small known peaks can be observed at 2.1, 3.1, 4.7, and 6.7 MeV along with other unknown peaks. It is not possible to comment on whether these are genuine peaks, given they are poorly defined.

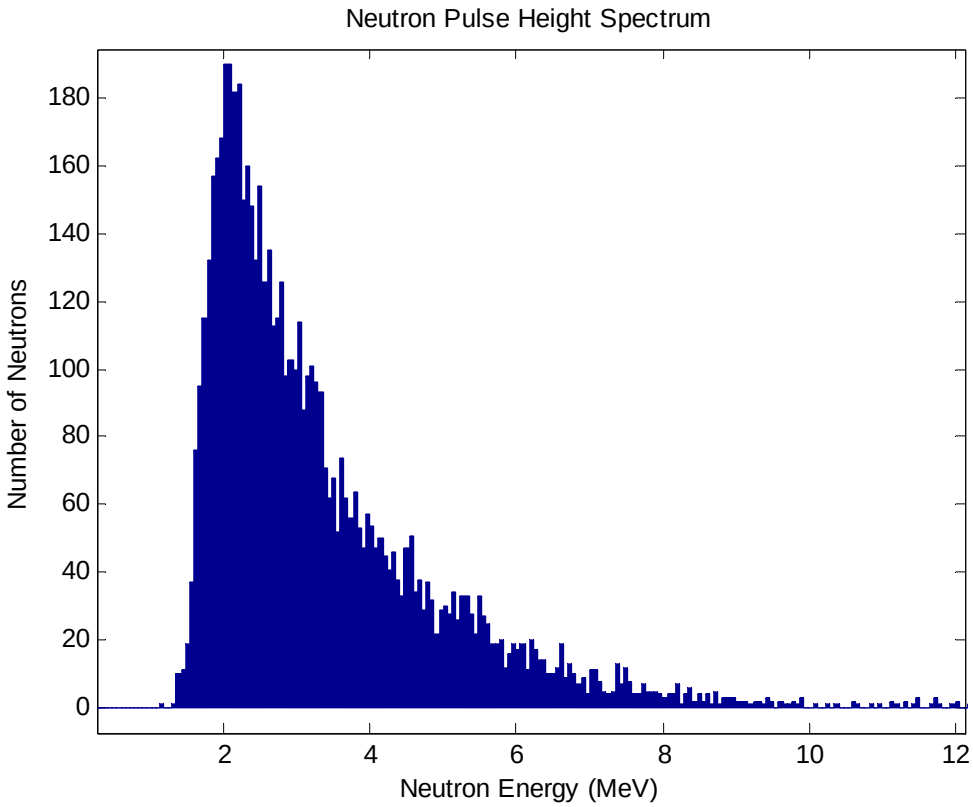

Fig. 25. PuBe neutron pulse height spectrum (128 channel) for the BC-523a detector.

5. Discussion

5.1 Evaluation of Reconstruction Algorithm

The agreement between the reconstructed data (using the neutron history algorithm) and the Lehman (1968) MCNP "transported" benchmark is good, considering the large number of factors that can alter both spectra (Fig. 26). The most obvious area where the two spectra deviate is in the region below 1.0 MeV. The benchmark increases rapidly due to the exponential increase in neutron absorption efficiency as neutron energy decreases. The experimental data falls off to zero around 0.5 MeV due to low-light scintillation pulses generated in the detector. Essentially, any neutron below 0.5 MeV will be indistinguishable from electronic noise. In the region above 7 MeV the relative error becomes large enough to make a comparison difficult, although it is encouraging that both spectra are bound by a similar upper limit of approximately 10.5 MeV. This larger error is a result of the relatively small number of neutrons that are absorbed by the BC-523a detector.

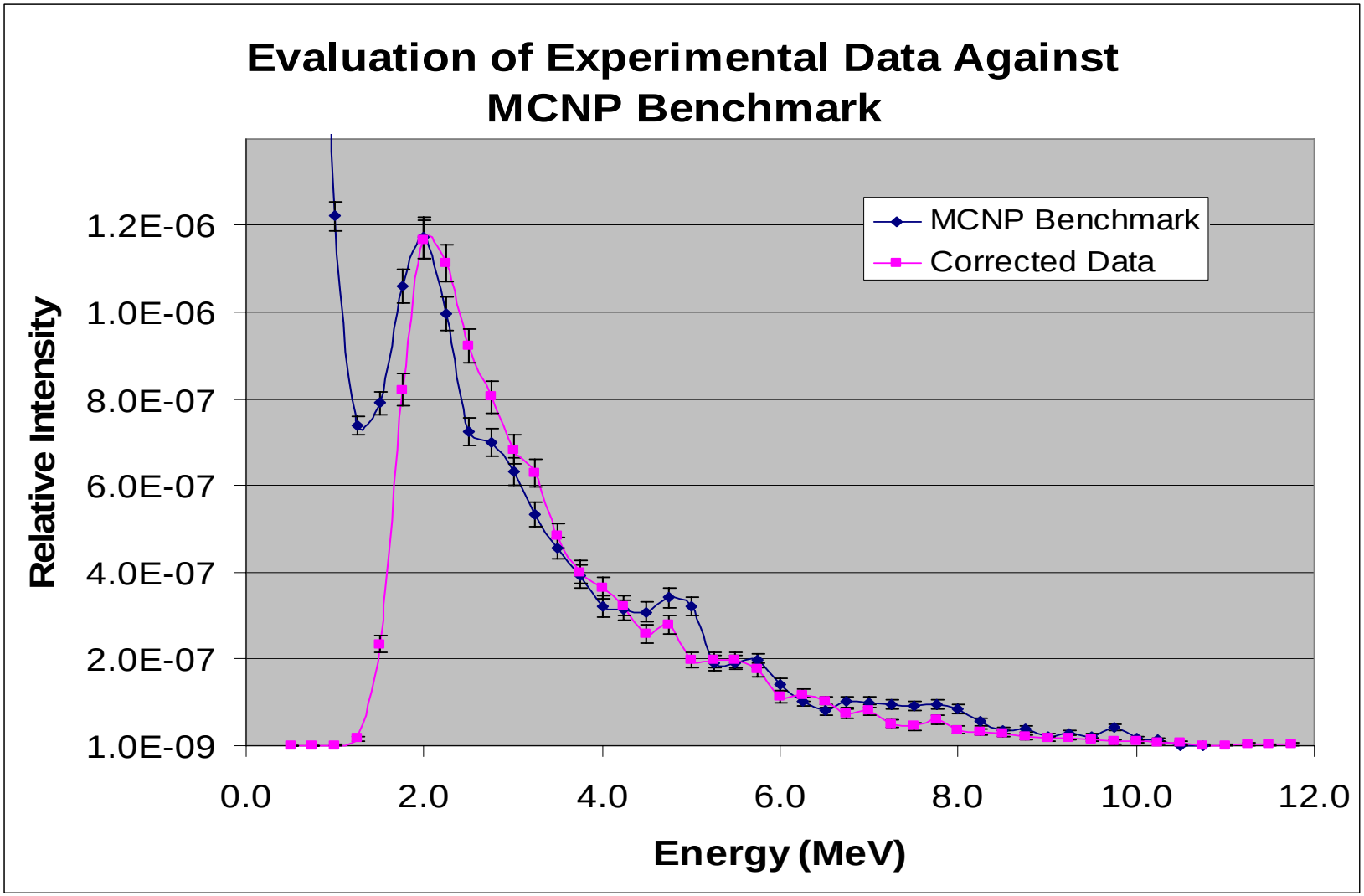

Fig. 26. Evaluation of experimental data against MCNP benchmark.

The other smaller deviations between the two spectra likely originate from two main sources:

(1) The Lehman benchmark data, itself, has inherent error. Furthermore, only the cement walls and wooden cradle for our detector were modeled. All other material in the laboratory will also have a thermalizing effect on the neutron spectrum, resulting in a degraded energy spectrum.

(2) The final major source of error is in the calibration factor that was implemented. Much of this work is based on Aoyama's previous work. Although the same detector type, size, and photomultiplier were used, their responses will not be identical. Furthermore, the gamma-ray calibration estimated response is based on locating a broad, poorly defined Compton edge. Both of these factors can result in less precise calibration values (recoil proton response function).

The results are nonetheless encouraging when they are compared to other potential calibration methods (Fig 27). If a linear calibration is used, based on the response of a 1 MeV neutron, then the calibration will underestimate response below 1 MeV and overestimate (by over an order of magnitude at 10 MeV) the response above 1 MeV. This is due to the non-linear light response of the scintillator upon absorption of recoiled proton energy. If it is assumed that the neutron undergoes only one collision before it is absorbed, one can see that the response above approximately 1 MeV is relatively close to the benchmark. This is a misleading result, however the single collision model is accurate only a small fraction of the time because the likelihood of only one collision occurring before absorption in boron is very small. A single collision correction will typically place neutrons at energies far below their

actual energy. This can be seen by examining the response below about 1 MeV, which exceeds the benchmark by nearly an order of magnitude.

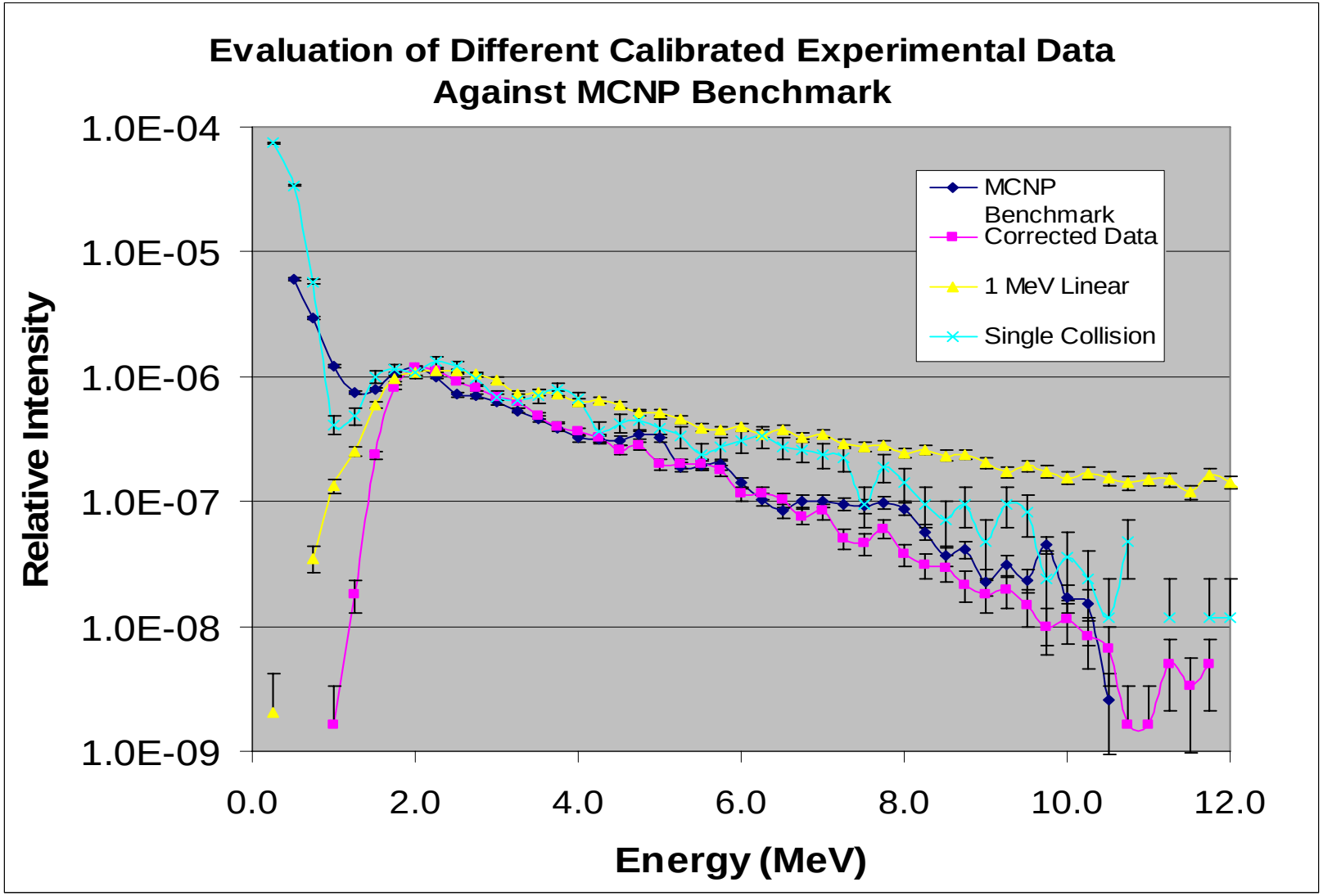

Fig. 27. Evaluation of different calibrated experimental data against MCNP benchmark.

5.2 Evaluation of Neutron/Gamma-Ray Separation Techniques

The neutron/gamma-ray pulse separation was less than ideal, primarily due to the relatively slow digitizer time. However, a broad criterion of a fast-to-total charge ratio of 0.8 was found as a somewhat reliable method for discrimination between gamma-rays and neutrons. It is encouraging, however, that the shape of the experimental neutron spectrum was very close to the benchmark given this poor neutron/gamma-ray separation. This suggests that the time gating (between the prompt and boron capture pulse) was sufficient to identify particles that deposit all of their energy within the active volume of the detector as neutrons. Therefore, any improvement in the separation of neutrons and gamma-rays by pulse-shape discrimination will only improve the false-positive rate of neutrons identified as depositing all of their energy in the active volume.

Likewise, it will be useful to have the ability to identify neutrons that do not deposit all their energy. If the digitizer sampling speed can be increased to 0.5 to 1 gigasample per second, the scintillation pulse can be characterized well enough for pulse-shape discrimination techniques to work well (D'Mellow 2007, Jastaniah 2003). This remains true as long as the prompt scintillation pulse amplitude is above approximately 150 keVee, given that no pulse-shape discrimination techniques work well below this pulse amplitude. If this work were to continue, and digitizer speed were increased, all of the pulse-shape discrimination techniques discussed in the literature review would need to be performed to see if one technique stood out as the most effective.

5.3 Cosmic Muon Discrimination

At the conclusion of this study the question of how best to discriminate cosmic muons remains unanswered. The background cosmic muon flux yields a relatively steady background count rate in all radiation detectors. Large organic detectors are particularly susceptible to this effect. The ultimate impact of this effect is application specific. Muon detection is more significant in low count rate applications. This effect is also significant in detection systems that are designed to identify more than one radiation type, such as the BC-523a system. If research with the BC-523a system is to continue to the level of an application specific detection system, then an appropriate technique to discriminate against cosmic muons must be pursued. Shielding a detector from cosmic muons is impractical given that the range of typical cosmic muons is several meters in lead. This leaves only two potential techniques for cosmic muon discrimination.

The first technique is a pulse-shape discrimination, very similar to the pulse-shape discrimination used in this research, to differentiate between neutrons and gamma-rays. In a scintillator, the ratio of fluorescence and delayed fluorescence light produced by ionizing radiation is dependent on the LET of the radiation. Cosmic muons have a unique LET relative to fast electrons (produced by gamma-rays) and recoiled protons (produced by neutrons). This results in a unique ratio of fluorescence and delayed fluorescence for cosmic muons that can be used for identification (Moszynski 1991).

The second technique for cosmic muon discrimination is to use a coincidence phoswich system. As muons move though material, their energy loss as a function of

distance traveled through the material is nearly constant. Assume a phoswich system is constructed in a manner in where the BC-523a material is surrounded by a suitable scintillation material (NaI, CsI, etc.). For such a system if a cosmic muon interacts with the inner scintillator, then the cosmic muon must also interact with the outer scintillator. This results in two distinct pulse components that can be used to identify the coincidence pulse generated by the cosmic muon. This is, essentially, how a classical cosmic muon veto system operates (Bernstein 2008). Furthermore, the path of a cosmic muon through some relatively small amount of material (such as a detector) will remain undeviated. The phoswich detector can be constructed in such a way that if a cosmic muon interacts with both scintillation materials, then the pathlengths through each scintillation layers will be proportional to each other. This will result in two simultaneous pulses, of proportional magnitude, which can be used to improve the fidelity of cosmic muon identification.

6. Conclusions

6.1 General System Performance Conclusions

The general performance of the BC-523a neutron spectroscopy system (and the associated neutron history reconstruction algorithm) is good. The Lehman (1968) data used as a benchmark was originally taken 40 years ago and required hundreds, if not thousands, of hours reviewing film to reconstruct the neutron spectrum of PuBe with an energy resolution of approximately 0.25 MeV. By contrast, the BC-523a system was able to collect a spectrum with higher energy resolution in a few hours and data processing required less than one minute.

The system can be deemed as preliminarily successful because it reproduced a very complicated neutron spectrum composed of both sharp peaks and gradual features. This is even more encouraging given that the experiment was performed in a small room, with a large number of gamma-ray check sources, and a relatively slow digital processor.

Perhaps most encouraging is the fact that the system may be capable of identifying sharp resonance peaks in the PuBe neutron source. This suggests that the system might have an energy resolution better than expected and that a more refined (faster sampling) BC-523a neutron spectroscopy system may be able to perform high-resolution, high-efficiency neutron spectroscopy.

6.2 Future Work

The next logical step in this line of research would be to further benchmark the neutron history reconstruction algorithm against known monoenergetic neutron

sources such as the 2.45 MeV and 14.1 MeV neutrons produced by the D-D and D-T fusion reactions, respectively. These experiments would further quantify the results of the neutron history reconstruction algorithm in terms of the overall energy accuracy and energy resolution.

Currently, the limiting factor in this BC-523a boron capture gated system is the relatively poor discrimination between neutrons and gamma-rays based on pulse shape discrimination alone (the system appears successful at discriminating between neutrons and gamma-rays based on the time gating technique). This poor discrimination is due to the poor characterization of the pulse shapes (primarily their fall time). This poor pulse characterization is directly related to the characteristics of the digitizer. While the resolution and bandwith of the digitizer are excellent, the relatively slow sampling time results in a statistically noisy quantification of the slow and fast components of the prompt scintillation pulse. If the sampling speed were to increase to 1 GS/s, the separation of neutrons and gamma-rays would improve dramatically, while still using the double charge integration method or exponential fit method (Marrone 2002), so long as the magnitude of the prompt scintillation pulse remains above 150 keVee.

Research on the use of pulse-shape analysis to discriminate neutrons from gamma-rays is extensive in organic scintillators. It has been well documented that any pulse-shape analysis technique used on pulses below approximately 150 keVee in magnitude yields poor separation (Guerrero 2008). This is caused by an increase in statistical noise, which deteriorates the characterization of the pulse shape. This effect results in false neutron positives in the presence of low energy gamma-ray fields.

Making any organic scintillator (including BC-523a) a poor substitute for the ^{3}He tube neutron detectors.

The greatest advantage of the ^{3}He detector is that it is essentially invisible to gamma-rays, given its low Z composition and low atomic density. This is an ideal characteristic for use in portal monitors and non-destructive assay systems, where gamma-ray fields can be strong and neutron false positives are detrimental.

A possible solution to the replacement of the ^{3}He detector is a phoswich detector with a core of liquid scintillator (BC-523a) surrounded by NaI. Sodium iodide has a very long decay time when compared to BC-523a, making it easy to discriminate between radiation interaction events that take place in the plastic scintillator versus NaI. If a neutron were to enter the detector it would be invisible to the NaI. If the neutron deposits enough energy in the plastic scintillator (a pulse above 150 keVee), then classic pulse-shape techniques can be used to identify the pulse as a neutron. However, if the pulse is below 150 keVee, then pulse-shape discrimination alone will not be sufficient for proper identification. The key to this phoswich detector is its potential ability to identify gamma-ray interactions that occur in the plastic scintillator volume. Due to the low Z nature of plastic scintillators, gamma-ray interaction will essentially all be Compton scattering events, resulting in a scattered photon leaving the plastic scintillator volume and entering the NaI volume. If the thickness of the NaI layer is chosen properly, it will absorb the majority of these scattered photons. If a low-energy pulse is recorded in the plastic scintillator volume, and simultaneously in the NaI volume, it is reasonable to say that the deposition in the liquid scintillator was the result of a gamma-ray interaction. If a low-energy pulse is

recorded in the plastic scintillator volume, and no interaction takes place in the NaI volume, it is reasonable to say that the pulse was the result of a neutron interaction. This will potentially result in a detector with excellent gamma-ray and neutron discrimination characteristics even at low deposition energies. The end result would be a system that is very sensitive to neutron and gamma-rays, has excellent discrimination characteristics, and is able to perform simultaneous spectroscopy on gamma-rays and neutrons. This phoswich configuration is also ideal for the cosmic muon discrimination techniques discussed in Section 5.3. These properties would make an ideal system for special nuclear material monitoring and non-destructive assay.

Ultimately, this line of research may lead to an "all-in-one" radiation measurement device. If the phoswich design above were to be augmented with a thin layer of a scintillating material with a scintillation time different that the other two scintillators (such as anthracene), the detector would also become sensitive to beta particles. A control system could be implemented via a field-programmable gate array (Farsoni 2006) to identify particle type and assign energy. The possibility exists that even the photomultiplier tube itself could be replaced by a solid state photodiode system (Renker 2006). The end result could be a low cost, low power consumption detector capable of simultaneous gamma-ray, beta particle, and neutron spectroscopy.

REFERENCES

Abdurashitov, J.; Garvin, V.; Kalikhov, A.; Matushko, V.; Shikhin, A.; Yants, V.; Zaborshaia, O.; Adams, J.; Nico, J.; Thompson, A. A high resolution, low background fast neutron spectrometer. *Nuclear Instruments & Methods in Physics Research, Sections A: Accelerators, Spectrometers, Detectors and Associated Equipment.* 476A: 318-321; 2002.

Aleksan, R.; Bouchez, J.; Cribier, M.; Kajfasz E.; Pichard, B.; Pierre, F.; Poinsignon, J.; Spiro, M.; Thomas, J. Measurement of fast neutrons in the Gran Sasso laboratory using a Li-6 doped liquid scintillator. *Nuclear Instruments & Methods in Physics Research, Sections A: Accelerators, Spectrometers, Detectors and Associated Equipment.* 274A: 203-206; 1989.

Anderson, M.E.; Neff, R.A. Neutron energy spectra of different size PuBe sources. *Nuclear Instruments & Methods*. 99:231-235; 1972.

Aoyama, T.; Honda, H.; Kudo, C.M.; Takeda, N. Energy response of a full-energy-absorption neutron spectrometer using boron-loaded liquid scintillator BC-523. *Nuclear Instruments & Methods in Physics Research, Sections A: Accelerators, Spectrometers, Detectors and Associated Equipment.* 333A: 492-501; 1993.

Batchelor, R.; Morrison, G. Helium-3 Neutron Spectrometers. *Fast neutron physics: part 1*. IIIC: 413-439; 1960.

Bernstien, A.; Bowden, N.S.; Misner, A.; Palmer, T.; Monitoring the thermal power of nuclear reactors with a prototype cubic meter antineutrino detector. *Journal of Applied Physics.* 103, 074905 (2008)

Bertin, A.; Bruschi, M.; Bysritsky, V.; Capponi, M.; Cereda, B.; D'Antone, I.; De Castro, S.; Galli, D.; Giacobbe, B.; Marconi, U.; Massa, I.; Moroni, C.; Piccinini, M.; Poli, M. Semprini-Cesari, N.; Spighi, R.; Stolupin, V.; Vecchi, S.; Vezzani, A.; Villa, M.; Vitale, A.; Wozniak, J.; Zavattini, G.; Zoccoli, A. Performance of a coincidence neutron spectrometer with double pulse-shape discrimination. *Nuclear Instruments & Methods in Physics Research, Sections A: Accelerators, Spectrometers, Detectors and Associated Equipment.* 337A: 445-460; 1994.

Bramblett, R.L.; Ewing, R.I.; Bonner, T.W.; *Nuclear Instruments & Method.* 9, 1 (1960)

Britvich, G.I.; Vasil'chenko, V.G., Gilitsky, Yu.V.; Chubenko, A.P.; Kushnireko, A.E.; Mamidzhanyan; E.A.; Pavluchenko, V.P.; Pikalov, V.A.; Romakhin, V.A.; Soldatov, A.P.; Sumaneev, O.V.; Chernichenko S.K.; Shien, I.V.; Shepetov, A.L. A neutron detector on the basis of a boron containing plastic scintillator. *Nuclear Instruments & Methods in Physics Research, Sections A: Accelerators, Spectrometers, Detectors and Associated Equipment.* 550A: 343-358; 2005.

Brooks, F.D.; Klien, H. Neutron spectroscopy-historical review and present status. *Nuclear Instruments & Methods in Physics Research, Sections A: Accelerators, Spectrometers, Detectors and Associated Equipment.* 476A: 1-11; 2002.

Colonna, N; Tagliente G. Response of liquid scintillator detectors to neutrons of $E_n < 1$ MeV. *Nuclear Instruments & Methods in Physics Research, Sections A: Accelerators, Spectrometers, Detectors and Associated Equipment.* 416A: 109-114; 1998.

Czirr, J.; Jenson, G. A compact neutron coincidence spectrometer, its measured response functions and potential applications. *Nuclear Instruments & Methods in Physics Research, Sections A: Accelerators, Spectrometers, Detectors and Associated Equipment.* 349A: 532-539; 1994.

Czirr, J.; Merrill, D.; Buehler, D.; McKnight, T.; Carroll, J.; Abbott, T.; Wilcox, E. Capture-gated neutron spectroscopy. *Nuclear Instruments & Methods in Physics Research, Sections A: Accelerators, Spectrometers, Detectors and Associated Equipment.* 476A: 309-312; 2002.

D'Mellow, D.; Aspinall, M.D.; Mackin, R.O.; Joyce, M.J.; Peyton, A.J. Digital discrimination of neutrons and gamma rays in liquid scintillators using pulse gradient analysis. *Nuclear Instruments & Methods in Physics Research, Sections A: Accelerators, Spectrometers, Detectors and Associated Equipment.* 578A: 191-197; 2007.

Ely, James; Kouzes, Richard; Schweppe, John; Siciliano, Edward; Strachan, Denis; Weier. The use of energy windowing to discriminate SNM from NORM in radiation portal monitors. *Nuclear Instruments & Methods in Physics Research, Sections A: Accelerators, Spectrometers, Detectors and Associated Equipment.* 560A:373-387; 2006.

Farsoni A. 2006. Simultaneous beta/gamma digital spectroscopy (dissertation). Corvallis (OR): Oregon State University.

Ferguson, A. Gas recoil counters. *Fast neutron physics: part 1.* IIA: 179-209: 1960.

Flaska, M.; Pozzi, S. Identification of shielded neutron sources with the liquid scintillator BC-501A using a digital pulse shape discrimination method. *Nuclear Instruments & Methods in Physics Research, Sections A: Accelerators, Spectrometers, Detectors and Associated Equipment.* 577A: 654-663; 2007.

Gilboy, W.B., Jenneson, P.M., Simons S.J.R., Stanley, S.J., Rhodes, D. Industrial radiography with cosmic-ray muons: A progress report. *Nuclear Instruments & Methods in Physics Research, Sections A: Accelerators, Spectrometers, Detectors and Associated Equipment.* 580A: 785-787; 2007.

Guerrero, C., Cano-Ott, D., Fernandez-Ordonez, M., Gonzalez-Romero, E., Martinez, T. Villamarin, D. Analysis of the BC501a neutron detector signals using the true pulse shape. *Nuclear Instruments & Methods in Physics Research, Sections A: Accelerators, Spectrometers, Detectors and Associated Equipment.* 597A: 212-218; 2008.

Howarth, P. High count rate performance of NE 213 scintillation detectors with associated pulse shape discrimination electrons. *Nuclear Instruments & Methods in Physics Research, Sections A: Accelerators, Spectrometers, Detectors and Associated Equipment.* 376A: 67-81; 1996.

Jastaniah, S.D.; Sellin, P.J. Digital techniques for n/gamma pulse shape discrimination and capture-gated neutron spectroscopy using liquid scintillators. *Nuclear Instruments & Methods in Physics Research, Sections A: Accelerators, Spectrometers, Detectors and Associated Equipment.* 517A: 202-210; 2003.

Johnson, C. Recoil Telescope Detectors. *Fast neutron physics: part 1* II.C: 247-295; 1960.

Jordan, K.; Gozani, T. Detection of U-235 in hydrogenous cargo with Differential Die-Away Analysis and optimized neutron detectors. *Nuclear Instruments & Methods in Physics Research, Sections A: Accelerators, Spectrometers, Detectors and Associated Equipment.* 579A: 388-390; 2007.

Jordanov, Valentin; Knoll, Glenn. Digital synthesis of pulse shape in real time for high resolution radiation spectroscopy. *Nuclear Instruments & Methods in Physics Research, Sections A: Accelerators, Spectrometers, Detectors and Associated Equipment*. 345A: 337-345; 1994.

Jordanov, Valentin; Knoll, Glenn; Huber, Alan; Pantazis. Digital techniques for real-time pulse shaping in radiation measurements. *Nuclear Instruments & Methods in Physics Research, Sections A: Accelerators, Spectrometers, Detectors and Associated Equipment* 353A: 261-264; 1994.

Kamykowski, E.A. Comparison of calculated and measured spectral response and intrinsic efficiency for a boron-loaded plastic neutron detector. *Nuclear Instruments & Methods in Physics Research, Sections A: Accelerators, Spectrometers, Detectors and Associated Equipment.* 317A: 559-566; 1992.

Klien, H.; Neumann, S.; Neutron and photon spectroscopy with liquid scintillation detectors in mixed fields. *Nuclear Instruments & Methods in Physics Research, Sections A: Accelerators, Spectrometers, Detectors and Associated Equipment.* 476A: 132-142; 2002.

Kudo, K.; Takeda, N. Energy response of a full-energy-absorption neutron spectrometer using boron-loaded liquid scintillator BC-523. *Nuclear Instruments & Methods in Physics Research, Sections A: Accelerators, Spectrometers, Detectors and Associated Equipment.* 333A: 492-501; 1993.

Lawrence, D.C. Mixed radiation dosimetry of a plutonium-beryllium neutron source. *Health Physics*. Vol. 7: 179-184; 1962.

Lee, J.H.; Lee C.S. Response function of NE213 scintillator for 0.5-6 MeV neutrons measured by an improved pulse shape discrimination. *Nuclear Instruments & Methods in Physics Research, Sections A: Accelerators, Spectrometers, Detectors and Associated Equipment.* 402A: 147-154; 1997.

Lehman, R.L. The origin of neutron groups in beryllium sources. *Nuclear Instruments & Methods.* 60: 253-260; 1968.

Lo Presti, Charles; Weier, Dennis; Kouzes, Richard; Schweppe, John. Baseline suppression of vehicle portal monitor gamma count profiles: A characterization study. *Nuclear Instruments & Methods in Physics Research, Sections A: Accelerators, Spectrometers, Detectors and Associated Equipment.* 562A: 281-297; 2006.

Marrone, S.; Cano-Ott, D.; Colonna, N.; Domingo, C.; Gramegna, F.; Gonzalez, E.M.; Ginsing, F.; Heil, M.; Kappeler, F.; Mastinu, P.F.; Milazzo, P.M.; Papaevangelou, T.; Pavlopoulos, P.; Plag, R.; Reifarth, R.; Tagliente, G.; Tain, J.L.; Wisshak, K. Pulse shape analysis of liquid scintillators for neutron studies. *Nuclear Instruments & Methods in Physics Research, Sections A: Accelerators, Spectrometers, Detectors and Associated Equipment.* 490A: 299-307; 2002.

Moszynski, M.; Bizard, G.; Costa, G.J.; Durand, D.; El Masri, Y.; Guillaume, G.; Hanappe, F.; Heusch, B.; Huck, A.; Peter, J.; Ring, Ch.; Tamain, B. Study of neutron-gamma discrimination by digital charge comparison method for a large volume liquid scintillator. *Nuclear Instruments & Methods in Physics Research, Sections A: Accelerators, Spectrometers, Detectors and Associated Equipment.* 317A: 262-272; 1992.

Muehlhaus, C. Neutron Detection by Reaction Induced in Scintillators. *Fast neutron physics: part 1.* III.B: 387-411:1960.

Neiler, J.; Good, W. Time-of-Flight Techniques. *Fast neutron physics: part 1.* IVA: 509-621; 1960.

Patronis, N.; Kokkoris, M.; Giantsoundi, D.; Perdikakis, G.; Papadopoulas, C.; Vlastou, R. Aspects of GEANT4 Monte-Carlo calculations of the BC501A neutron detector. *Nuclear Instruments & Methods in Physics Research, Sections A: Accelerators, Spectrometers, Detectors and Associated Equipment.* 578A: 351-355; 2007.

Reeder, P.; Peurrung, A.; Hansen, R.; Stromswold, D.; Hensley, W.; Hubbard, C. Detection of fast neutron in a plastic scintillator using digital pulse processing to reject gammas. *Nuclear Instruments & Methods in Physics Research, Sections A: Accelerators, Spectrometers, Detectors and Associated Equipment.* 422A: 84-88; 1999.

Renker, D. Geiger-mode avalanche photodiodes, history, properties, and problems. *Nuclear Instruments & Methods in Physics Research, Sections A: Accelerators, Spectrometers, Detectors and Associated Equipment.* 567A: 48-56; 2006.

Saint-Gobain Crystals a division of Saint-Gobain Ceramics & Plastics, Inc., a subsidiary of Compagnie de Saint-Gobain headquartered in Paris, France. http://www.detectors.saint-gobain.com/Media/Documents/S0000000000000001004/SGC_BC523A_Data_Sheet.pdf

Siciliano, E.R.; Ely, J.H.; Kouzes R.T.; Milbrath; B.D.; Schweppe; J.E.; Stromswold; D.C. Comparison of PVT and NaI(Tl) scintillators for vechicle portal monitor applications. *Nuclear Instruments & Methods in Physics Research, Sections A: Accelerators, Spectrometers, Detectors and Associated Equipment.* 550A: 647-674; 2006.

Slaughter, D.; Accatino, M.; Bernstien, A.; Biltoft, P.; Church, J.; Descalle, M.; Hall, J.; Manatt, D.; Mauger, G.; Moore, T.; Norman, E.; Petersen, E.; Pruet, J.; Prussin, S. The nuclear car wash: A system to detect nuclear weapons in commercial cargo shipments. *Nuclear Instruments & Methods in Physics Research, Sections A: Accelerators, Spectrometers, Detectors and Associated Equipment.* 579A: 349-352; 2007.

Wang, J.; Galonsky, A.; Kruse, J.; Zecher, P.; Deak, F.; Horvath, A.; Kiss, A.; Seres, Z.; Ieki, K.; Iwata, Y. Neutron cross-talk in a multi-detector system. *Nuclear Instruments & Methods in Physics Research, Sections A: Accelerators, Spectrometers, Detectors and Associated Equipment.* 397A: 380-390; 1997.

Zecher, P.; Galonsky, A.; Carter, D.; Seres, Z. Neutron/gamma-ray pulse-shape discriminator. *Nuclear Instruments & Methods in Physics Research, Sections A: Accelerators, Spectrometers, Detectors and Associated Equipment.* 508A: 434-439; 2003.

Appendices

Appendix A-Matlab Control Program

```
%load data.mat;
%For 200 mhz digitar aka sample every 5 ns
pulses=double(pulses);
gamma=1; %initializing gamma-ray counter
neutron=1; %initializing neutron counter for neutrons with an energy
associated with them
totalneutron=1; %initializing total neutron counter
p=1; %initalizing pulse counting
gammaenergy=0; %initializing gammaenergy
calfactor=0.291; %calibration factor for gamma ray (keV/ALU)
for count=2:26123 %data set
    Xw=pulses(count,:); %taking data one row at a time
    y=Xw;
    intfilter=[(ones(1,24)*+1),(ones(1,24)*-1)]; %integrating filter
    fastfilter=[(ones(1,5)*+1),(ones(1,5)*-1)];
    boronfilter=[(ones(1,5)*+1),(ones(1,5)*-1)];
    int=conv(y,intfilter);
    fastint=conv(y,fastfilter);
    boronint=conv(y,boronfilter);
    totalcharge=max(int(100:500));
    fastcharge=max(fastint(100:500));
    boroncharge=max(boronint(130:360));
    ratio=(fastcharge/totalcharge);
    if ratio >=0.80  %this value is the gamma/neutron slow decay ratio
cut off
        gamma=gamma+1;
        gammaenergy=totalcharge*calfactor;
    end
    if ratio <=0.80
        totalneutron=totalneutron+1;
    end
    if ratio <=0.80 && 50<boroncharge && 150>boroncharge %boron capture
pulse is detected
        neutron=neutron+1;
        %LNE=int/19.8; %linear calibrated neutron energy for 9.8 MeV
peak
        %UNE=0.0097*(int^0.667); %uncorrected neutron energy (single
collision)
        INE=0.0279*(totalcharge^0.6615); %Initial neutron energy
reconstruction method imperical fit
         ANE=INE/(.62); %actual neutron energy
         %uncorrectedneutronspec(neutron)=UNE;
         neutronscint(neutron)=totalcharge*calfactor; %neutron pulse in
keVee
         initialneutronspec(neutron)=INE;
         neutronspec(neutron)=ANE; %storage array for neutron spectrum
         neutronratio(neutron)=ratio; %makes and array of ratios for
"qualified neutrons"
         %neutronfast(neutron)=peakfastdecay
         %neutronslow(neutron)=peakslowdecay
    end
%     subplot(2,2,1)  %plotting functions for individual pulses
%     plot(y)
%     title('Single Peak Anode Voltage vs. Time')
%     xlabel('Time Step (5ns/step)')
%     ylabel('Output Voltage')
```

```
%     subplot(2,2,2)
%     plot(fastdecay(90:150))
%     title('Fast Scintiallation Filtered Pulse')
%     xlabel('Time Step (5ns/step)')
%     ylabel('Output Voltage')
%
%     subplot(2,2,3)
%     plot(slowdecay(90:150))
%     title('Slow Scintiallation Filtered Pulse')
%     xlabel('Time Step (5ns/step)')
%     ylabel('Output Voltage')
%
%     subplot(2,2,4)
%     plot(boronpulsedecay(140:365))
%     title('Boron Capture Scintiallation Filtered Pulse')
%     xlabel('Time Step (5ns/step)')
%     ylabel('Output Voltage')

     p=p+1;
     %peakfastdecayarray(p,:)=peakfastdecay;  %pulseheight spectrum for
all pulses
     gammaratio(gamma,:)=ratio; %array of gamma-ray ratios
     gammaspec(gamma,:)=gammaenergy; %pulseheight spectrum for gamma-
rays only
     boroncapturepulsespec(p,:)=boroncharge;
end

[n,xout]=hist(neutronspec,64);

% subplot(2,2,1)
% hist(uncorrectedneutronspec,64);
% title('Uncorrected Neutron Pulse Height Spectrum')
% xlabel('Neutron Energy (MeV)')
% ylabel('Number of Neutrons')
%
% subplot(2,2,2)
% hist(initialneutronspec,64)
% title('Initial Neutron Pulse Height Spectrum')
% xlabel('Neutron Energy (MeV)')
% ylabel('Number of Neutrons')

% subplot(1,1,1)
% hist(gammaspec,128)
% title('Gamma-ray Pulse Height Spectrum')
% xlabel('Gamma-ray Energy (keV)')
% ylabel('Number of Gamma-ray')

subplot(1,1,1)
hist(neutronspec,120)
title('Neutron Pulse Height Spectrum')
xlabel('Neutron Energy (MeV)')
ylabel('Number of Neutrons')

%final particle counts
gamma-1;
```

```
totalneutron-1;
neutron-1;
```

Appendix B-MCNP Codes

Boron Capture detector with 14.2 MeV neutrons (collisional and inelastic scatter photon losses)

```
1  1  -2.7     -6 1 -2    imp:p,n=1
2  1  -2.7     -6 3 -4    imp:p,n=1
3  1  -2.7     2 -3 5 -6  imp:p,n=1
4  2  -.916    2 -3 -5    imp:p,n=1
5  3  -.00127  -8 #1 #2 #3 #4  imp:p,n=1
6  0           8          imp:p,n=0

1 px 1
2 px 1.127
3 px 8.747
4 px 8.874
5 c/x 0 0 6.35
6 c/x 0 0 6.477
7 px .5
8 so 20

mode n p

m1 13027 1
m2 1001 4.98  6012 2.86  8016 .811  5010 .243  5011 .027
m3 7014 .8  8016 .2
m4 1001 1
m5 6012 1
m6 8016 1
m7 5010 1
m8 5011 1
sdef erg=14.2 sur=7 dir=1 rad=d1 pos=0 0 0
si1 0 6.35
sp1 -21 0
f4:n 4
fm4 .0498  4  -3 $hydrogen total elastic rate
f14:n 4
fm14 .0498  4  102 $hydrogen n,gamma rate
f104:n 4
fm104 .0286 5  -3 $carbon elastic scatter rate
f114:n 4
fm114 .0286 5  -2 $carbon total absorption rate
f124:n 4
fm124 .0286 5  102 $carbon (n,gamma) rate
f134:n 4
fm134 .0286 5  103 $carbon (n,p) rate
f144:n 4
fm144 .0286 5  104 $carbon (n,d) rate
f154:n 4
fm154 .0286 5  107 $carbon (n, alpha) rate
f204:n 4
fm204 .00811 6  -3 $oxygen elastic scatter rate
f214:n 4
fm214 .00811 6  -2 $oxygen total absorption rate
f224:n 4
fm224 .00811 6  102 $oxygen (n,gamma) rate
f234:n 4
fm234 .00811 6  103 $oxygen (n,p) rate
f244:n 4
```

```
fm244 .00811 6  104 $oxygen (n,d) rate
f254:n 4
fm254 .00811 6  107 $oxygen (n, alpha) rate
f304:n 4
fm304 .00243 7  -3 $b-10 elastic scatter rate
f314:n 4
fm314 .00243 7  -2 $b-10 total absorption rate
f324:n 4
fm324 .00243 7  102 $b-10 (n,gamma) rate
f334:n 4
fm334 .00243 7  103 $b-10 (n,p) rate
f344:n 4
fm344 .00243 7  104 $b-10 (n,d) rate
f354:n 4
fm354 .00243 7  107 $b-10 (n, alpha) rate
f404:n 4
fm404 .00027 8  -3 $b-11 elastic scatter rate
f414:n 4
fm414 .00027 8  -2 $b-11 total absorption rate
f424:n 4
fm424 .00027 8  102 $b-11 (n,gamma) rate
f434:n 4
fm434 .00027 8  103 $b-11 (n,p) rate
f444:n 4
fm444 .00027 8  104 $b-11 (n,d) rate
f454:n 4
fm454 .00027 8  107 $b-11 (n, alpha) rate
f504:p 4            $total gamma flux produced
e504  0 1999i 20
f8:p 4              $pulse height tally or gammas absorbed
e8  0 1999i 20
nps 2.5e8
```

PuBe neutron transport in laboratory

```
c     cell cards
1     2 -0.916    1 -2 -10 imp:p,n=1           $bc-532a detector
2     3 -11.6     -20      imp:p,n=1           $lead shield
99    1 -1.2e-3   -60 #1 #2  imp:p,n=1    $air volume
999   0  60  imp:p,n=0                         $void

c     surface card
1  px 50     $surface of the face of the detector
2  px 57.62  $surface of the back of the detector
10 cx 6.35   $outside cylinder of the detector
20 so 5      $lead shield around PuBe source
30 box -105 -180 -180  210 0 0  0 360 0  0 0 360
40 box -135 -210 -210  270 0 0  0 420 0  0 0 420
50 box -300 -300 -180  600 0 0  0 600 0  0 0 360
60 box -310 -310 -190  620 0 0  0 620 0  0 0 380

c    information card
mode n
sdef pos=0 0 0  erg=d1  wgt=1
```

```
si1  0 0.25 0.5 0.75 1.0  1.25 1.5  1.75 2.0 2.25 2.5 2.75 3.0 3.25 3.5
3.75 4.0  4.25 4.5 4.75 5.0 5.25 5.5 5.75 6.0 6.25 6.5 6.75 7.0 7.25
7.5  7.75  8.0 8.25 8.5 8.75 9.0 9.25 9.5 9.75 10  10.25 10.5
sp1  0 0 3.5 3.2  2.75 2.15 2.35 2.35 2.8 4.2  4.0 3.1  4.4 6.75 7.1
4.45 4.45 4.45 5.0 6.4  6.4 4.45 4.2 4.0  2.7 1.8  1.6 2.3  2.0 2.15
2.15 2.6 2.6 1.6  1.0 1.0  0.5 0.8  0.8 1.1  0.9 0.4   0.4
f4:n 1
e4 0 1e-8 0.25 0.5 0.75 1 1.25 1.5 1.75 2 2.25 2.5 2.75 3 3.25 3.5 3.75
4 4.25 4.5 4.75 5 5.25 5.5 5.75 6 6.25 6.5 6.75 7 7.25 7.5 7.75 8 8.25
8.5 8.75 9 9.25 9.5 9.75 10 10.25 10.5 10.75
fm4 .00243 5 -2
f6:n 1
e6 0 1e-8 0.25 0.5 0.75 1 1.25 1.5 1.75 2 2.25 2.5 2.75 3 3.25 3.5 3.75
4 4.25 4.5 4.75 5 5.25 5.5 5.75 6 6.25 6.5 6.75 7 7.25 7.5 7.75 8 8.25
8.5 8.75 9 9.25 9.5 9.75 10 10.25 10.5 10.75
m1 7014 0.8  8016 0.2 $air
m2 1001 4.98  6012 2.98  8016 0.811  5010 0.243  5011 0.027 $bc-523a
m3 82000 1 $Pb
m4 1001 2  8016 1 $water
mt4 lwtr
m5 5010 1 $pure boron 10
m6 1001 8.48e-2  8016 6.04e-1  11023 9.47e-3  12000 2.99e-3  13027
2.48e-2
        14000 2.42e-1  19000 6.86e-3  20000 2.05e-2  26054 2.74e-4
        26056 4.26e-3  26057 9.76e-5  26058 1.30e-5
ctme 30
```

Intrinsic efficiency of BC-523a

```
c     cell cards
1     4 -0.916    1 -2 -10 imp:n=1           $bc-532a detector
99    0    -99 #1 imp:n=1    $air volume
999   0  99  imp:n=0                          $void

c     surface card
1  px 100
2  px 107.62
10 cx 6.35
99 so 200

c    information card
mode n
sdef pos=0 0 0  erg=2.5  wgt=1
f4:n 1
e4  0 .00001 1023i 10
fm4 .00243 8 -2
m1 7014 0.8  8016 0.2 $air
m4 1001 4.98  6012 2.98  8016 0.811  5010 0.243  5011 0.027 $bc-523a
m8 5010 1 $pure boron 10
ctme 5
```

Modeling of 482 keV photons

```
c     cell cards
1     2 -0.916    1 -2 -3  imp:p=1     $bc-523a detector
99    1 -1.2e-3   -99 #1   imp:p=1    $air volume
999   0  99  imp:p=0                    $void

c     surface card
1  px 0
2  px 7.62
3  cx 6.35
99 so 50

c    information card
mode p
sdef pos=0 0 0 erg=0.482 pos=0 0 0 cell=1 rad=d1 ext=d2 axs=1 0 0 wgt=1
SI1= 0 6.35
SI2= 7.62
f8:p 1                          $small BC-523a tally
e8 0 .001 4094i 4.096
m1 7014 0.8  8016 0.2 $air
m2 1001 4.98  6012 2.98  8016 0.811  5010 0.243  5011 0.027 $bc-523a
ctme 60
```